Radionuclide Imaging of Children

27

Reza Vali, Susan McQuattie, and Amer Shammas

27.1 Introduction

Although many types of radionuclide studies are similar in adults and children, there are specific consideration to be aware of in the pediatric population. Nuclear medicine physicians and technologists are often faced with frightened children and anxious parents, and as such careful planning and good communication is essential. Having the appropriate tools, environment, and enough time is of pivotal importance to acquire an optimum study. In addition, it is important to be aware of the normal variances and appropriate thresholds in order to interpret an activity as abnormal in children as compared with adults. In this chapter we review the common nuclear medicine procedures in children, focusing on the indication of the study, patient preparation, dose of the radioactivity, and the interpretation of the studies. Similar to the previous edition, the effective radiation doses listed are for a 20-kg 5-year-old child except where indicated.

It should be noted that the protocols suggested in the following pages are institutional specific and may vary to some degree from those currently in practice in other pediatric facilities. As with any nuclear medicine procedure, it is beneficial to consult local regulations and guidelines such as the EANM, SNMMI, and Image Gently Alliance when establishing pediatric specific protocols.

27.2 Genitourinary System

Radionuclide studies of the genitourinary system are perhaps one of the most common procedures in children. There are various clinical indications in pediatric nephro-urology imaging including:

- Cortical imaging of acute pyelonephritis, scars, and infarction
- Evaluation of congenital anomalies (duplication and ectopia)
- Assessment of the renal function in hydronephrosis (suspected ureteropelvic junction or ureterovesical junction obstruction) or after renal trauma
- Evaluation of renal transplant
- GFR studies
- Evaluation of vesicoureteral reflux

Most nuclear medicine studies in genitourinary system disorders can be categorized into three main groups:

1. Evaluation of renal function (including both glomerular and tubular studies)

R. Vali (✉) · S. McQuattie · A. Shammas
Nuclear Medicine, The Hospital for Sick Children, University of Toronto, Toronto, ON, Canada
e-mail: reza.vali@sickkids.ca

H. Ahmadzadehfar et al. (eds.), *Clinical Nuclear Medicine*,
https://doi.org/10.1007/978-3-030-39457-8_27

2. Evaluation of renal cortex
3. Evaluation of the bladder

Other radionuclide studies such as scintigraphy of the testis, evaluation of tumors (e.g., MIBG scan for neuroblastoma), etc. can also be seen in pediatric population. This section will focus on the most common radionuclide studies in pediatric nephro-urological disorders.

27.3 Dynamic Renography

Similar to the adults, dynamic renal imaging is generally acquired after intravenous injection of a glomerular radiotracer [e.g., ^{99m}Tc-diethylene triamine pentaacetic acid (DTPA)] or a tubular agent [e.g., ^{99m}Tc-mercaptoacetyltriglycine (MAG3) and ^{99m}Tc-ethylenedicysteine (^{99m}Tc-EC)]. In children 2 years of age and younger (because of immature nephrons and low GFR), ^{99m}Tc-MAG3 is the preferred radiotracer due to its better quality and higher target-to-background activity. However, when GFR measurement is of interest, ^{99m}Tc-DTPA should be used. Similar protocols can be used for both ^{99m}Tc-DTPA and ^{99m}Tc-MAG3 renal scans (Box 27.1).

Box 27.1 Protocol Summary for Dynamic Renography

Indications

To evaluate renal function and to distinguish between retention in the calyceal system due to obstruction and a dilated system without mechanical obstruction.

Contraindication

None. However, it is better to postpone the study or interpret with caution in the first 2 weeks of age.

Patients sensitive to sulfonamides may also be sensitive to furosemide.

Patient Preparation

Make sure the patient doesn't have any contraindication to furosemide administration.

If the patient has a cardiac disease, prophylactic antibiotic may be needed prior to urethral catheterization (consult with the cardiologists). Hydration fluid volume may need to be modified to guard against fluid overload.

Hydration: Via IV, hydrate the child with normal saline. Give 10 cc per kg if the child is under 6 months and 15 cc per kg if over 6 months. Allow half of the total volume to infuse 15 min prior to the MAG3 injection—the other half can infuse during the image acquisition. Older, compliant children can be given oral hydration. Record the total amount of hydration on the requisition.

Have the child void just prior to the scan if he/she is not catheterized.

Radiopharmaceutical

^{99m}Tc-DTPA, 3.7 MBq (100 μCi)/kg; minimum, 20–37 MBq (1 mCi)∗.

^{99m}Tc-MAG3, 1.9 MBq (50 μCi)/kg; minimum, 15–37 MBq (1 mCi)∗.

Effective dose (mSv/MBq): 0.015 for ^{99m}Tc-MAG3 and 0.012 for ^{99m}Tc-DTPA [1].

Image Acquisition

Position the patient supine with the bladder at the bottom of the field of view.

Acquire serial 30–60 s images (64 × 64 or 128 × 128 matrix) for 30–60 min, depending on the technique chosen.

Acquire 1–3 min dynamic images after upright positioning (child sit up or have the parent hold a baby upright for about 5–15 min). Late PM images acquired after 60 min are also useful in certain cases.

Processing and Analysis

Please refer to the text for more detailed processing in different methods of Lasix injection. Renogram, DRF, T max, T½ of the furosemide curve, PM images after the upright positioning or at 60 min, and NORA are useful parameters for interpretation.

∗EANM (2) suggests a minimum activity of 15 MBq for ^{99m}Tc-MAG3 and 20 MBq for ^{99m}Tc-DTPA. The minimum activity is 37 MBq for both radiotracers according to the SNM guideline (3).

PM, post-micturition; DRF, differential renal function; T max, time of maximum activity; NORA, normalized residual activity.

The child should be hydrated before the study (Box 27.1). Urinary catheterization is suggested in younger children to allow for free flow of urine from the bladder during the study. Catheterization may not be necessary for older and compliant children. However, it is especially useful when there is history of vesicoureteral reflux, severely dilated pelvicalyceal system, and suspected UVJ obstruction or in patients with a pelvic kidney. Children undergoing renal scintigraphy in conjunction with GFR measurement are not routinely catheterized; however, a post-void image is taken where possible.

Patient preparation and the technique of scanning are summarized in Box 27.1. Similar to adults, a few seconds after the administration of the radiotracer, both kidneys are visualized symmetrically (flow or perfusion phase). Evaluation of perfusion phase is important in patients with hypertension or after renal transplantation. Within 1–3 min the activity accumulates in both kidneys' parenchyma (extraction, uptake or cortical phase). The uptake phase is perhaps one of the most important phases of a renal scan. The cortical uptake in the first 1–3 min is used to evaluate the differential renal function (DRF). It is important to pay attention to the region of interest (ROI) over the kidneys and background activity particularly on follow-up scans (to be consistent). In the case of a poor renal function, or when the kidney is not located in the normal position, evaluation of the DRF is more accurate with a renal cortical radiotracer such as ^{99m}Tc-DMSA. Excretion of the radiotracer starts very early but will be more prominent within a few minutes after injection (excretory phase). The tracer then clears from the kidneys into the ureters and bladder gradually (drainage or clearance phase).

Furosemide (1 mg/kg IV; maximum 40 mg) is commonly used to distinguish between retention in the calyceal system due to obstruction and a dilated system without mechanical obstruction. The pelvicalyceal system may be dilated due to congenital malformation, vesicoureteral reflux, previous obstruction, and bladder abnormalities, such as neurogenic bladder or posterior urethral valve (PUV), rather than a current mechanical obstruction. A number of different protocols exist in terms of the timing of furosemide injection; however the results of all protocols are similar. Some centers inject furosemide when the dilated renal pelvis is maximally distended with radiotracer. Injection of furosemide 20 min after the radiotracer administration (F+20) is more common in adult centers. The F+20 method has the advantage in that the diuretic will be injected only if there is retention in one of the kidneys. In our institution furosemide is injected immediately after the radiotracer administration (F-0). The F-0 method has the advantage of a shorter acquisition time, and no need for a separate injection. Furosemide can also be injected 15 min before the radiotracer administration [2].

A renogram (time–activity curve that represents the cortical uptake, excretion, and drainage of the kidneys over time) is drawn by placing a ROI over the kidneys and background. Some descriptive parameters are useful to interpret a renogram. The time to reach the peak of activity in the parenchyma is called T max which is normally about 2–5 min after radiotracer administration. Typically, an ROI over the collecting system that excludes the renal parenchyma is used in adults to evaluate the diuresis phase. However, in the pediatric population, especially in small children, it is difficult and perhaps not very accurate to exclude the parenchyma. Thus, in practice, a similar ROI to that which is drawn for the evaluation of cortical uptake is used for the assessment of diuresis. If there is evidence of hydroureter, another ROI can be drawn to include the ureters. T½ which is the time that the activity in the collecting system reaches 50% of the maximum activity is commonly used to assess the drainage or clearance of the collecting systems. Normalized residual activity (NORA) which is the ratio of the residual activity in the kidney at time *t* (over a period of 1 min) to time 1–2 min is also a useful parameter to evaluate the drainage of the kidney [2]. In many cases, post-upright positioning images, post-micturition (PM) image, and

delayed images (e.g., at 60 min) are of pivotal importance to assess the obstruction and the prognosis (Fig. 27.1).

T½ is normally used with furosemide. In case of a mechanical obstruction, the drainage of the calyceal system may be delayed by the narrowed area, and the T½ is prolonged. Therefore, the time–activity curve may show minimal or no evidence of downsloping. On the other hand, in a nonobstructive system, the drainage is improved

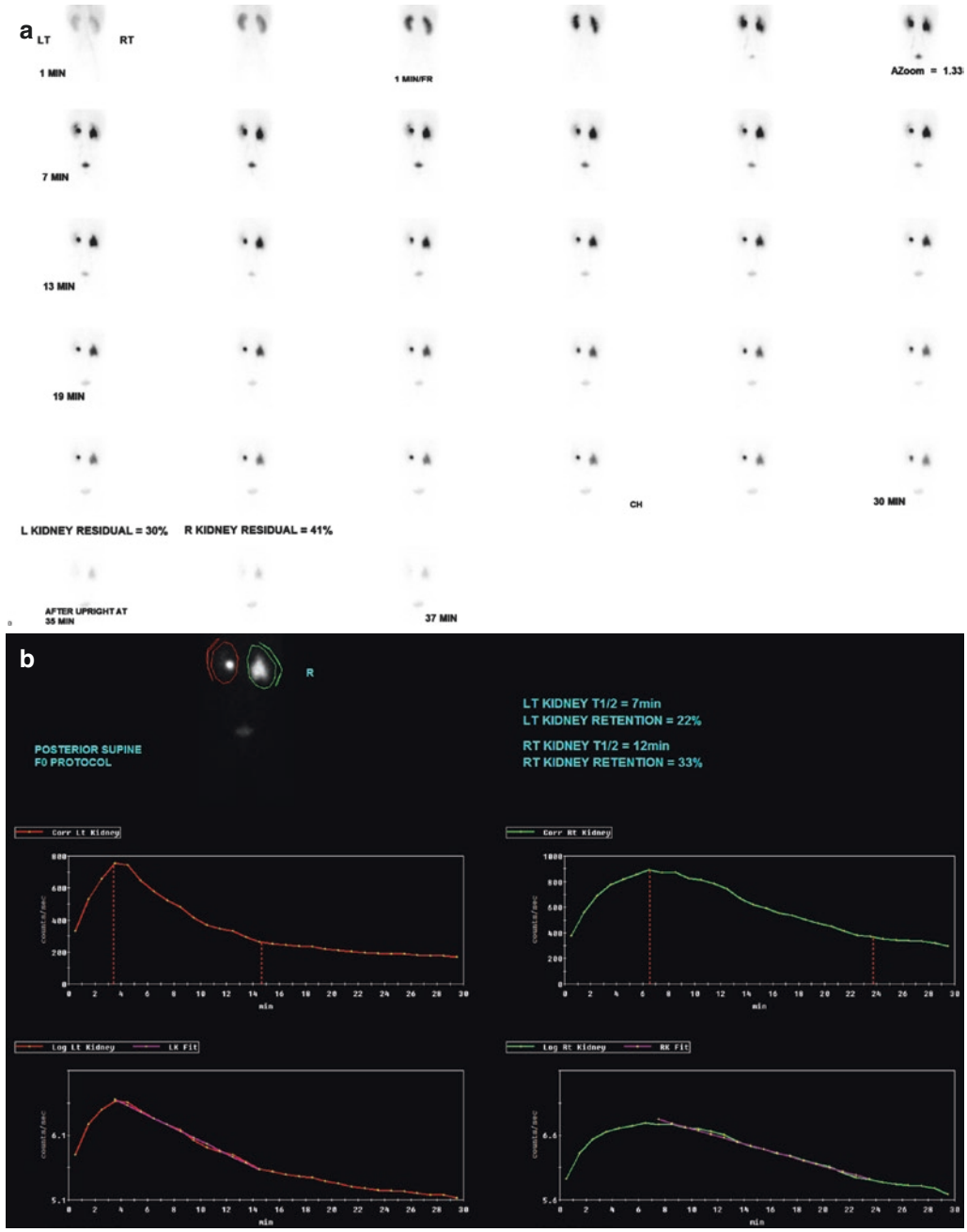

Fig. 27.1 Renal scan with ^{99m}Tc-MAG3 in a 2-year-old child with prominent left renal pelvis and dilated right pelvicalyceal system on ultrasound. There is mild retention of activity in the right pelvicalyceal system (**a**) with a T½ of 12 min (**b**). There is further drainage of the activity on both sides after the upright positioning (**a**) with no evidence of mechanical obstruction

after administration of furosemide. In general, if the T½ values are less than 10 min, the study is accurate to exclude obstruction. Alternatively, if the T½ is markedly prolonged, the study is suggestive of high-grade obstruction. For values in between, the T½ is relatively equivocal, and other clinical parameters or follow-up is needed to confirm or exclude a mechanical obstruction. In uncomplicated cases (e.g., preserved cortical function), if there is no evidence of a high-grade obstruction, a close follow-up may be the best approach for equivocal T½ [4]. This is particularly true in neonatal hydronephrosis as the natural behavior of hydronephrosis is variable and may change over time [3].

There are other conditions in which the interpretation of drainage values should be done cautiously. For example, if furosemide is injected at 20 min and the radiotracer has already cleared from the kidney, the T½ after the injection of furosemide is invalid as the collecting system has been already emptied. In large hydronephrotic kidneys (pelvic volume greater than 75 mL), there will be a delay in clearance of the activity due to a dilution effect, even with no significant mechanical obstruction. Finally, in cases of poor renal function, the drainage of the kidneys cannot be accurately evaluated due to delayed accumulation of the activity within the kidneys. In other words, with incomplete input, evaluation of kidney output is not so reliable. Moreover, in severely decreased renal function response to the furosemide, stimulation is not optimum.

27.4 Renal Cortical Imaging

^{99m}Tc-DMSA (dimercaptosuccinic acid) is the radiotracer of choice for the assessment of renal cortex. ^{99m}Tc-DMSA is bound to proximal tubular cells with 40–65% of the injected dose present in the cortex 2 h after injection. Image acquisitions are usually obtained 2–3 h after the injection of 1.85 MBq/kg (0.05 mCi/kg) of ^{99m}Tc-DMSA (minimum dose 18.5 MBq) (Box 27.2). This study consists of two sets of acquisitions—one set, using the LEHR collimator, provides images for calculation of the differential function, and the other set, using the pinhole collimator or SPECT, provides multi-projection images for high-resolution assessment of the renal cortex. In our institute we acquire SPECT for patient older than 5 years. In some institutes SPECT images are obtained for the patients older than 1–3 years. Pinhole images are obtained in posterior and posterior oblique views. For the renal transplant patients, imaging should be acquired in anterior and oblique views. For pelvic kidney the anterior and anterior oblique views should be added to the acquired images of the normally positioned posterior kidney.

Box 27.2 Protocol Summary for DMSA

Indications

To evaluate for renal scarring, acute pyelonephritis, differential renal function, solitary or ectopic renal tissue, horseshoe kidney, space-occupying lesions, renal trauma, and hydronephrosis.

Contraindication

None. If there is any nuclear medicine scan performed in the last 24–48 h, it is better to postpone the study if possible.

Patient Preparation

No special requirements. Patients should have normal hydration—oral hydration is encouraged. Prior to imaging, patient should void or diaper is changed.

Radiopharmaceutical

^{99m}Tc-DMSA, 1.85 MBq/kg or 0.05 mCi/kg; minimum dose 18.5 MBq or 0.5 mCi.

Effective dose (mSv/MBq): 0.039 [12].

Image Acquisition

Image the patient 2–4 h following injection. If there is poor renal function, delayed imaging (up to 24 h) is useful.

Image the patient in anterior and posterior projection with a low-energy high-resolution collimator for 500k or 2 min for calculation of the differential function.

Continue with planar pinhole imaging (for younger children) or SPECT acquisition

(for older children) for high-resolution assessment of the renal cortex.

Pinhole imaging: For 8 min or 100k counts per view in posterior and posterior oblique projections for each kidney separately. The pinhole collimator should be within the same distance from patient for both kidneys.

SPECT acquisition: 128 matrix, 64 images, 180°; step and shoot 20 s/frame; zoom as required.

Processing and Analysis

Depending on the camera and the available software: for ordered subset expectation maximization (OSEM), use Butterworth filter with 0.52 critical frequency or Hanning filter with high cutoff smoothing kernel. Motion correction or attenuation correction can be done if needed.

The normal finding is the homogeneous uptake of the radiotracer in both kidneys with no definite focal cortical defect. The shape of the kidneys may be variable. There is usually mild decreased activity over the area of the pelvicalyceal system. Upper lateral region of the left kidney may be flattened due to splenic impression (Fig. 27.2). Indentations in the border of the kidneys may be seen due to fetal lobulation. The normal differential function is in the range of 43–57% for each kidney.

In addition to the usual indication of ^{99m}Tc-DMSA renal scan in acute pyelonephritis and detection of renal scars, it can also be helpful in the assessment of functioning cortical tissue in a dysplastic or small kidney, to evaluate the differential renal function, to evaluate ectopic kidney and horseshoe kidney, and to differentiate the hypertrophic columns of Bertin versus a tumor.

^{99m}Tc-DMSA can be helpful in evaluating a child with febrile UTI to evaluate for acute pyelonephritis. Recently, some authors have suggested to start with a DMSA scan when approaching a patient with acute pyelonephritis (the so-called top-down approach) instead of a radionuclide cystography due to the relative importance of renal damage rather than reflux in these patients [6]. Acute pyelonephritis shows as a single or multifocal area of decreased DMSA activity without volume loss or may present as a diffuse decrease in radiotracer activity (Fig. 27.3a). Reduced cortical activity after an episode of acute pyelonephritis may completely resolve within several months or may lead to a permanent scar formation (Fig. 27.3b). A follow-up ^{99m}Tc-DMSA study (at least 6 months after the acute pyelonephritis) is useful to detect scarring [7].

^{99m}Tc-DMSA scans are also useful to evaluate kidneys in other conditions. In ectopic kidneys, unlike intravenous pyelogram (IVP) and ultrasound, bowel gas or bony structures cannot obscure the ectopic kidney. ^{99m}Tc-DMSA can be helpful to distinguish renal ectopia from hypoplasia or agenesis. A DMSA scan is useful to evaluate function of the horseshoe kidney and also function of each moiety in a duplex kidney.

27.5 Radionuclide Cystography

Vesicoureteral reflux (VUR) is seen in approximately 1–2% of the pediatric population and up to 40% in children with acute pyelonephritis. Almost half of the patients with VUR diagnosed before birth or at neonate show spontaneous resolution by the age of 2–3 years. Thus, frequent imaging may be needed in some patients. In general, radionuclide VUR studies are indicated for evaluation at diagnosis (for females), for siblings of patients with reflux, and for follow-up studies in both females and males. For males or those patients with a suspicion of anatomic abnormalities, it is suggested to start with radiographic voiding cystography (VCUG) due to anatomical resolution [8]. In contrast to VCUG, continuous recordings during radionuclide cystography (RNC) with no extra patient radiation can increase the sensitivity and higher detection rate for the intermittent reflux. Quantification of the bladder volume at initiation of reflux and measurement of the residual bladder volume after voiding are other parameters that are useful for follow-up studies.

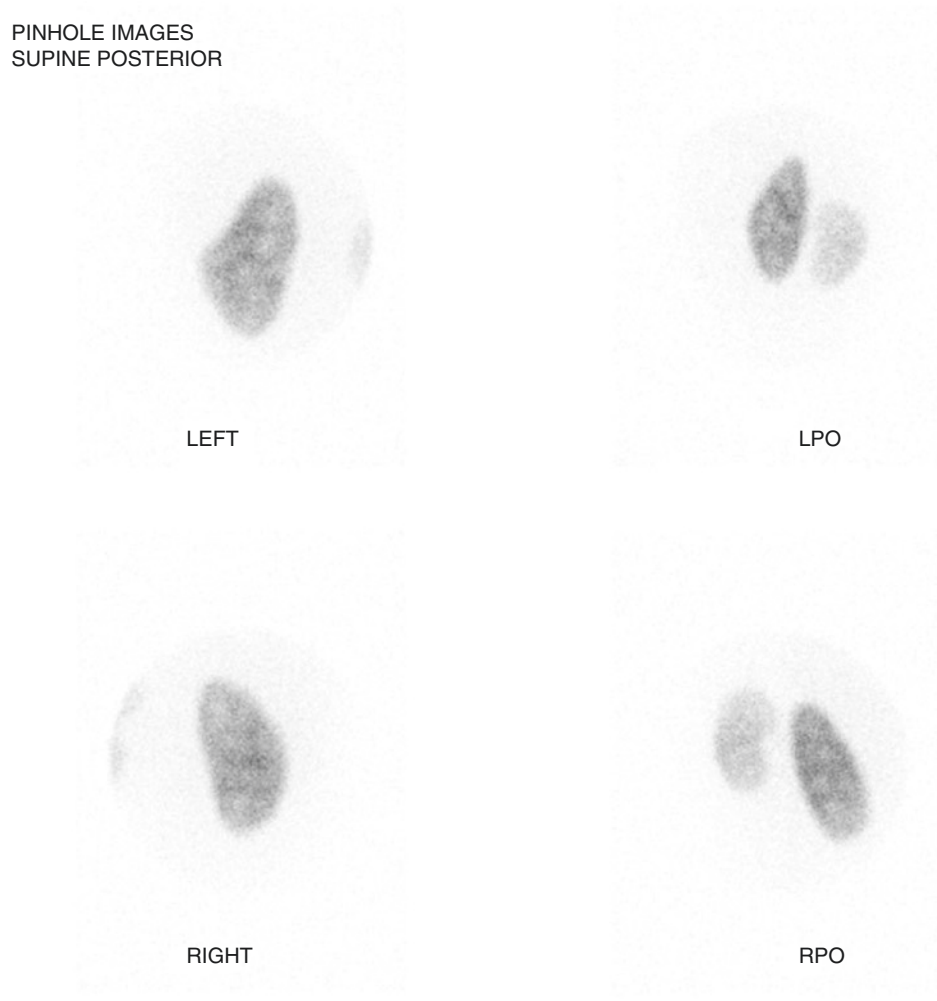

Fig. 27.2 Splenic impression: ^{99m}Tc-DMSA scan in a 4-year-old child with history of urinary tract infection. No definite focal cortical defect or loss of volume is visualized to suggest scarring. There is a flattening in the upper lateral region of the left kidney due to splenic impression

In direct radionuclide cystography (DRC), ^{99m}Tc-pertechnetate or ^{99m}Tc-sulfur colloid (total maximum dose is 37 MBq; 1 mCi) is infused into the bladder with saline via a urinary catheter. The filling phase can be completed when the optimum pre-estimated volume is achieved, when the patient has spontaneously voided, or when the flow from the bottle of solution is stopped in a non-voiding patient (back-pressure effect), and finally when bilateral severe reflux is visualized (the last one is controversial) [5]. Pre-estimated volume is calculated based on this formula: (age in years + 2) × 30 cc = bladder volume. For patients less than 1 year, the same formula is used (if the patient is 6 months old, the age will be 0.5) or is calculated based on this formula: weight in kg × 7 cc = bladder volume. Second or third attempts at filling the bladder may be considered if the target volume is not achieved.

The acquisition starts with filling of the bladder, and when reflux is noted, the bladder volume should be recorded. A single-head camera with a large FOV all-purpose collimator is used for imaging (for newborn less than 1 year, a converg-

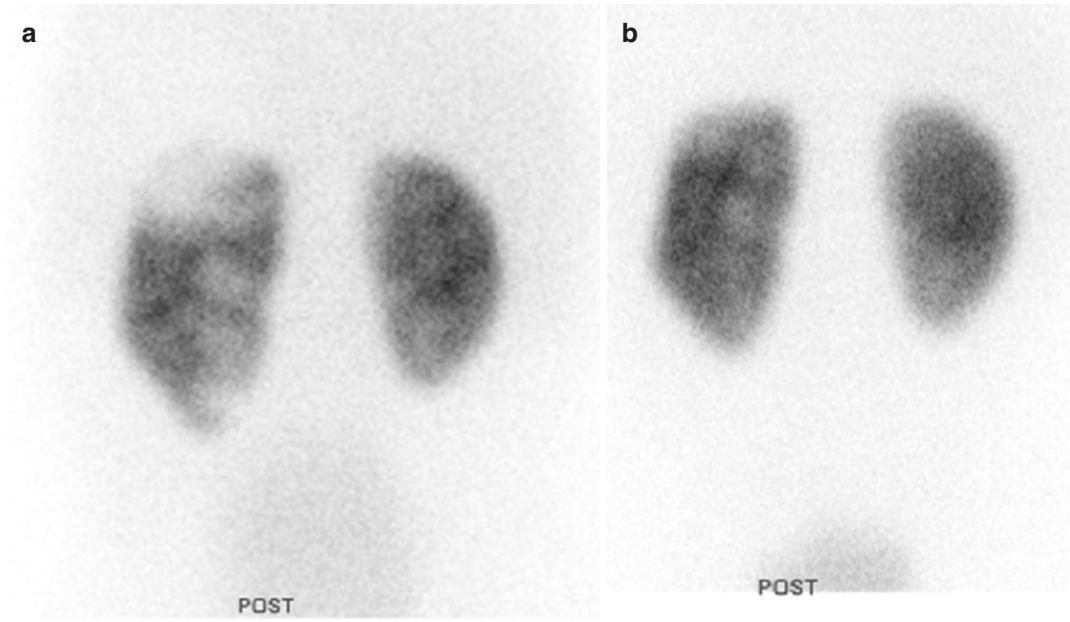

Fig. 27.3 Acute pyelonephritis: ^{99m}Tc-DMSA scan (posterior view) in a 12-month-old girl with fever showed a geographic photopenic defects in the upper and lower poles of the left kidney (**a**). Complete interval resolution of the photopenic defects was noted on follow-up scan 8 months later (**b**)

ing collimator is usually preferred). The acquisitions include dynamic imaging (128 matrix, 10 s/frame for 200 frames) during filling phase, continued with dynamic imaging (2 s/frame for 2 min) during voiding phase and a static post-void imaging (for 1 min). Presence of activity in the ureters or renal pelvis suggests VUR.

The grading system of RNC is different from VCUG. Grade 1 (or mild) reflux in RNC is the visualization of the activity in the ureter (equal to grade 1 in VCUG), a grade 2 (or moderate) is the visualization of activity in the collecting system (equal to grades 2 and 3 in VCUG), and grade 3 (or severe) is the visualization of activity in the collecting system with a dilatation of the collecting system and ureter (equal to grades 4 and 5 in VCUG) (Fig. 27.4).

Another method to detect vesicoureteric reflux is indirect radionuclide cystography (IRC). After a ^{99m}Tc-DTPA or MAG3 renal scan, when the radioisotope has completely cleared from the upper urinary tract and accumulated in the bladder, the child is asked to void and the reflux is assessed. This method has the advantages of additional information about the renal function, there is no need for catheterization, and it is more physiological (avoiding bladder overfilling) [9]. However, the sensitivity of the study is less than DRC or VCUG. Moreover, the patient should be cooperative and toilet trained (usually >3 years old), and the radiation dose is higher than DRC (Box 27.3).

Box 27.3 Protocol Summary for DRC

Indications

To evaluate for vesicoureteral reflux (evaluation of girls at diagnosis, siblings of patients with reflux, and for follow-up studies).

Contraindication

If the child has an active UTI, catheterization may be deferred until after treatment. Please follow your institutional policy for catheter instillation.

Patient Preparation

No special requirements. However if the patient has history of cardiac disease, then prophylactic antibiotics may be necessary. The referring physician is responsible for prescribing the antibiotics and must be informed at the time of booking.

Radiopharmaceutical

^{99m}Tc-SC administered via catheter: 18.5–37 MBq (0.5–1 mCi).

Effective dose (mSv/MBq): 0.0024 [5].

Image Acquisition

Dynamic imaging (128 matrix, 10 s/frame for 200 frames) during filling phase, continued with dynamic imaging (2 s/frame for 2 min) during voiding phase and a static post-void image (for 1 min).

Single-head, large FOV all-purpose collimator (for newborn less than 1 year, a converging collimator) is usually preferred.

Processing and Analysis

Typical evaluation of DRC is visual, reviewing the dynamic imaging for detection of reflux and measuring the bladder volume at the time of reflux. Measurement of the post-residual bladder volume is also helpful.

27.6 Gastric Emptying

A gastric emptying scan is a noninvasive and physiologic imaging technique to measure gastric emptying and to assess response to medication or surgery on the upper GI tract. A barium study is useful for evaluation of anatomic abnormalities. However, barium studies do not provide quantitative measurements and are not completely physiologic. Patients with delayed gastric emptying may present with nausea, vomiting, early satiety, epigastric fullness, or failure to thrive. Patients with diabetes, pyloric stenosis, duodenal stenosis, duodenal web, SLE, dermatomyositis, polymyositis, myotonic dystrophy, hypokalemia, acidosis, hypothyroidism, vagotomy, and gastric inflammation/infection and neurologically impaired children may have delayed gastric emptying. Certain clinical conditions such as partial gastric resection, damage to the vagus nerve, Zollinger–Ellison syndrome, carcinoid syndrome, and duodenal ulcer may

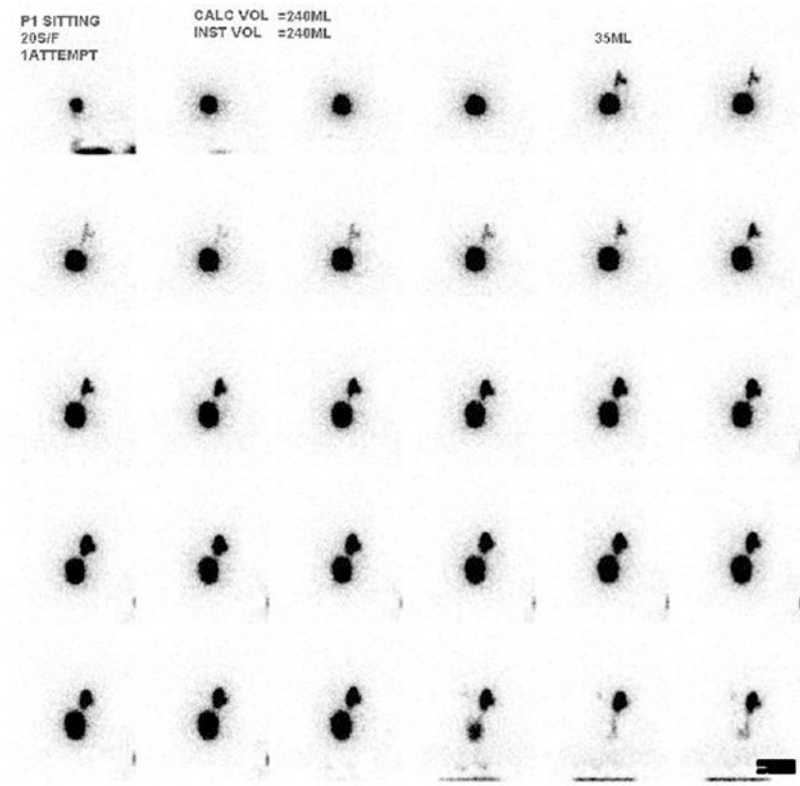

Fig. 27.4 Vesicoureteral reflux: direct radionuclide cystography in a 6-year-old child with history of pyelonephritis. Reflux of the tracer into the right dilated pelvicalyceal system (grade: severe) is noted during filling phase (at 35 cc filling). There is also reflux of the tracer into the left renal pelvis (grade: moderate) visualized during voiding

accelerate the gastric emptying. Medications may also affect the gastric emptying. Opioid or anticholinergic medications may delay gastric emptying, while cisapride, metoclopramide, erythromycin, and ondansetron may accelerate it.

Many factors affect the rate of gastric emptying. Liquid meals usually empty faster than solid meals with an exponential clearance of activity. Solid meals usually empty after a lag phase period followed by a relatively linear pattern. Higher fat content and calorie, increased osmolality, and larger particles may slow gastric emptying. A standardized meal (content, volume, and calories) is necessary to obtain a reliable study but can sometimes be challenging in children.

Milk or formula is usually used to measure gastric emptying in infants (the so-called milk scan). In a milk scan, gastroesophageal reflux and pulmonary aspiration can also be evaluated. The patient should be fasting for 2–4 h before the study. The volume of feed to be given to the child is determined in consultation with the child's physician, dietitian, or parent. The aim is to fill the stomach as much as the patient can tolerate. The milk is mixed with ^{99m}Tc-SC (sulfur colloid) since it remains stable in the acidic environment of the stomach and cannot be absorbed from the GI mucosa. ^{99m} Tc-SC (9.0 MBq; 0.25 mCi) is mixed in 50–75% of the liquid meal (radioactive or "hot" milk) with the remainder to be given "cold" (nonradioactive). The "hot" feed is followed by the "cold" liquid in order to clear the activity from the esophagus. The liquid should be administered in less than 10 min either orally, via NG (nasogastric) or G (gastric) tube. Imaging is performed immediately after the "feeding" phase is finished. The patient is imaged for 60 min using a dynamic acquisition (two consecutive sets of 30 min), 64 matrix, 5 s/frame. Infants are held upright between images, and older children are encouraged to sit up or walk between images. As the milk study is usually done in younger children, a posterior view acquisition is adequate (for solid gastric emptying, anterior and posterior acquisitions for a dual-head camera; anterior or left anterior oblique view for a single-head camera). Static posterior view acquisitions for 1 min (128 matrix) are suggested at 60 and 120 min. Although there is a range of normative values for a milk study in children, in our practice the study is considered to be normal if the half time of emptying is more than 50% at 1 h for children over the age of 2 and more than 50% at 2 h for children less than 2.

An egg sandwich (120 cc white egg) containing ^{99m}Tc-sulfur colloid (9.0 MBq; 0.25 mCi) with two pieces of white bread toasted, two packets of strawberry jam, and 120 mL of water is usually used for the solid gastric emptying study. The geometric mean activity (by simultaneously obtaining anterior and posterior images) is used to overcome the variability of counts with the posteroanterior migration of gastric contents during the acquisition. This is particularly important in older and obese children. If a single-head camera is used, left anterior oblique acquisition is the preferred projection. Static images (with an LEHR collimator and 128 matrix) for 1 min are acquired immediately after feeding (time 0) and at 30, 60, 120, and 240 min. There is limited information available for the normative values of different solid meals among different age groups of children. In young children the normal gastric emptying is 24–48% at 60 min and 48–70% at 120 min [11]. The normal values for adults, where the upper limits of normal range for gastric retention are 90%, 60%, 30%, and 10%, 1 h, 2 h, 3 h, and 4 h after ingestion of a meal, respectively [12], may be useful as a guide for older children (Box 27.4).

Box 27.4 Protocol Summary for Gastric Emptying Study

Indications

Nausea, vomiting, early satiety, epigastric fullness, or failure to thrive.

Contraindication

Food allergy to peanut butter or egg.

Patient Preparation

NPO for 4–6 h. Medications that delay gastric emptying, such as opiates or antispasmodic agents and prokinetic agents such as metoclopramide, tegaserod, domperidone, and erythromycin, are generally stopped 2 days before the test unless the test is done to assess the efficacy of these

drugs. Other medications that may have an effect on the rate of gastric emptying include anticholinergic agents atropine, calcium channel blockers, antacids, somatostatin progesterone, octreotide, theophylline, benzodiazepine, and phentolamine. Barium swallow study should not be performed within 72 h prior to this procedure.

Radiopharmaceutical

For solid study, ^{99m}Tc-SC egg white sandwich (120 cc) with water: 9 MBq (0.25 mCi).

For liquid study, ^{99m}Tc-SC (9 MBq; 0.25 mCi) is mixed in 50–75% of the liquid meal (radioactive or "hot" milk) with the remainder to be given "cold" (nonradioactive).

Effective dose (mSv/MBq): 0.024 [5].

Critical organ: proximal colon [12].

Image Acquisition

For liquid study, the patient is imaged for 60 min dynamic acquisition (two sets of 30 min) (with a low-energy high-resolution collimator and 64 matrix), 5 s/frame followed by static posterior view acquisitions for 1 min (128 matrix) at 60 and 120 min. Posterior view is adequate.

For solid study, static images (with a low-energy high-resolution collimator and 128 × 128 matrix) for 1 min are acquired immediately after feeding (time 0) and at 30, 60, 120, and 240 min. Obtain a simultaneous anterior and posterior views with a dual head camera and left anterior oblique view with a single-head camera.

Processing and Analysis

A region of interest is drawn over the stomach in different times. Background subtraction and radioactive decay correction should be performed.

27.7 Pulmonary Aspiration

Pulmonary aspiration can be seen in patients with congenital malformations of the head and neck (e.g., cleft palate) or after upper aerodigestive tract surgery or in neurologically impaired children. The patient may present with recurrent pneumonia. A liquid gastric emptying study (milk scan) and salivagram may be used for the assessment of the pulmonary aspiration in children.

Reviewing the images in a milk scan is helpful to detect gastroesophageal reflux (GER) as well as pulmonary aspiration. The technique is similar to the milk scan with the addition of a delayed static view (with a low-energy high-resolution collimator and 128 matrix for at least 5 min) of the chest added to the typical protocol. A milk scan can detect the aspiration related to GER (retrograde events). The detection rate of aspiration varies in different studies and is relatively low (up to 25%) [13]. The low detection rate of aspiration by a milk study is perhaps due to the low concentration of radiotracer and faster clearance of the radiotracer from the esophagus and stomach in some patients. Protective mechanisms such as cough reflex and mucociliary action can also reduce the sensitivity of the milk scan to detect pulmonary aspiration. Moreover, if the mechanism of pulmonary aspiration is an antegrade aspiration, it can be missed by a milk scan which is based on a retrograde aspiration detection. However, a milk scan has the advantage of evaluating the gastric emptying, GER, and pulmonary aspiration in one study.

A salivagram is a simple, noninvasive study used to evaluate pulmonary aspiration due to antegrade aspiration. The radiation dose is minimal (0.05 mSv) [14], and there is no specific preparation required for the study. The detection rate for this study is higher than a milk study. Since the frequency of antegrade reflux events as a cause of aspiration may be higher than that of retrograde reflux, particularly in neurologically impaired children, the sensitivity of a salivagram is higher than the milk scan. The higher concentration of radiotracer in a salivagram comparing with a milk scan is probably another reason for the higher sensitivity. In a study by Baikie et al. on 63 children with severe spastic quadriplegic cerebral palsy, the salivagram was most frequently positive (56%). Barium video-fluoroscopy was positive in 39%, and milk scan was positive in 6% of the cases [15].

In a salivagram, a drop of liquid containing a small amount of radioactivity (11 MBq; 0.3 mCi of ^{99m}Tc-SC) in 0.1 mL of saline is placed in the oral cavity usually under the tongue. Dynamic images (128 matrix, 30 s for 30 frames) followed by static images of the chest (one in posterior and one lateral projections for 5 min each with 256 matrix) are acquired immediately after administration of the radiotracer. After 5–10 min, 1 cc of water can be placed under the patient's tongue to promote mixing of the saliva in the mouth (this is controversial as it may change a salivagram into a swallow study). The pulmonary aspiration (antegrade aspiration) is diagnosed if there is evidence of tracheobronchial visualization or pulmonary aspiration. In general, the acquisition time is completed by 60 min. However, in the majority of cases, evidence of aspiration is seen in the first 15 min. The acquisition can be continued until the oral radioactivity is no longer present.

27.8 Gastroesophageal Reflux Study

Gastroesophageal reflux (GER) can be detected by pH probe. Reduced pH level over longer than standardized references values for age is often suggestive of an acid reflux event. The PH probe has the benefit of detecting late prandial reflux of nocturnal episodes of reflux. However, it is an invasive procedure and may have false negative results (due to elevation of pH by milk during the test). A milk scan is a physiologic, noninvasive, and simple study to detect GER especially in infants. In infants, the symptoms of GER are usually nonspecific and cannot reliably be used to diagnose GERD or predict the response to treatment. These symptoms include recurrent regurgitation with/without vomiting, symptoms related to pulmonary aspiration, and weight loss or inadequate weight gain. In older children and adolescents, a history and physical examination may be enough to make a diagnosis. Detection of non-acid reflux is another advantage of a milk scan which is reported in approximately 16% of children with GER [16]. The technique of a milk scan is described before. Visual dynamic review of computer-enhanced images is used to assess reflux. The number of episodes of reflux, the duration of each episode, the level reached within the esophagus, and the timing (early versus late) are the parameters that should be reported (Fig. 27.5).

27.9 Meckel's Diverticulum Scan

Meckel's diverticulum is the most common congenital abnormality of the small intestine (1–3% of the population). It is a true diverticulum caused by an incomplete closure of the omphalomesenteric duct. Meckel's diverticulum contains heterotopic gastric mucosa in as many as 50–60% of the cases; these patients usually present with bleeding and/or abdominal pain. Intermittent and painless bleeding per rectum is usually seen in patients less than 2 years old but may occur at any age. In certain cases, the ulceration of the diverticulum or adjacent small bowel mucosa may cause pain with or without bleeding. Other complications include perforation of the small bowel, partial or complete small bowel obstruction, and Meckel's diverticulitis.

Ultrasound is the first investigation to exclude other causes of abdominal pain or bleeding. However, Meckel's diverticulum may be missed in ultrasound or small bowel contrast radiography. ^{99m}Tc scintigraphy is a noninvasive common procedure for the diagnosis of Meckel's diverticulum containing heterotopic gastric mucosa. Approximately 25% of the administered activity accumulates in gastric mucosa. A focal uptake in the abdomen, commonly in the right lower abdomen, increasing over time at a rate similar to the gastric uptake is suggestive of a Meckel's diverticulum containing heterotopic gastric mucosa (Fig. 27.6). The sensitivity and specificity of a Meckel's scan to detect a Meckel's diverticulum are about 85% and 95%, respectively [17].

The patient should be fasted for 2–4 h as the lesion may be obscured by a full stomach or bladder. If possible, the study should be postponed for a few days after a barium study, or a radionuclide scan (Box 27.5). Certain procedures on GI (such as colonoscopy) or some medications (e.g., ethosuximide) may cause nonspecific uptake of the radioisotope due to bowel irritation and inflammation. Potassium perchlorate should not be used as it can reduce the uptake in the heterotopic gastric mucosa.

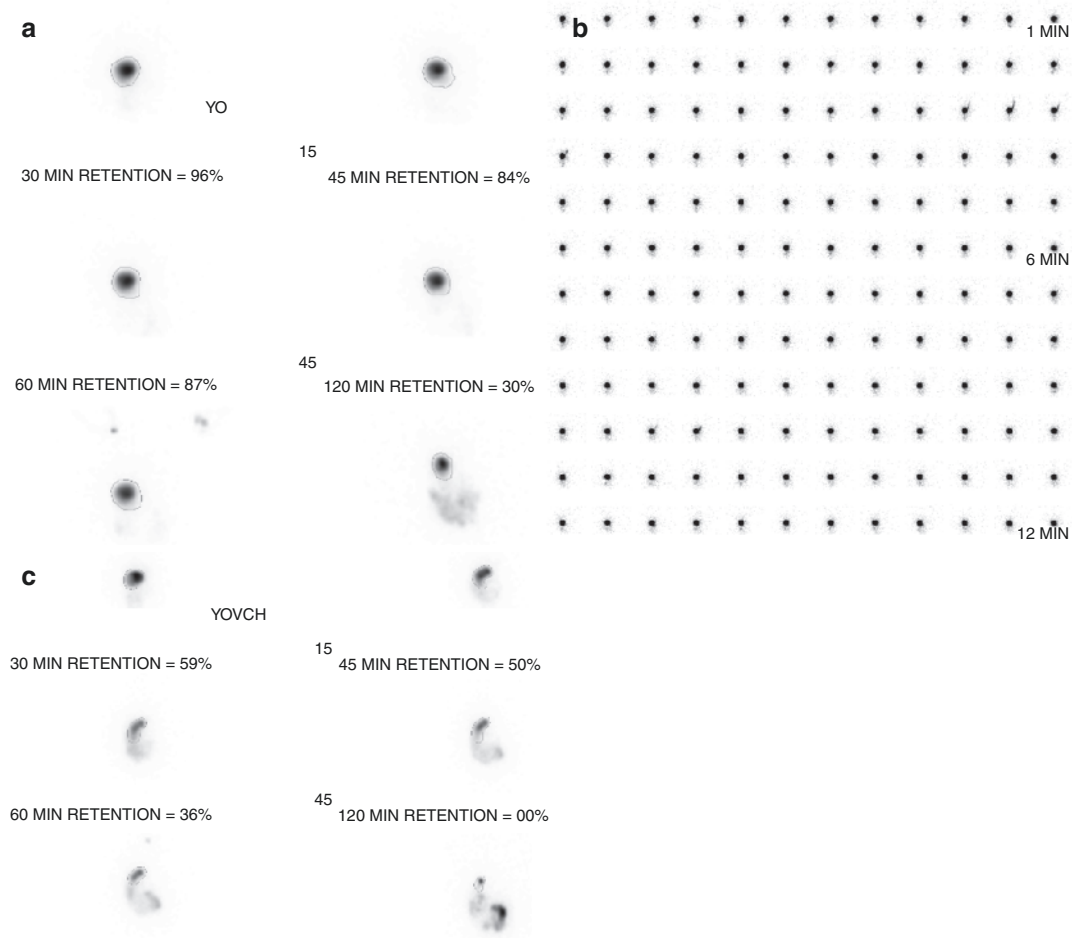

Fig. 27.5 Delayed gastric emptying with gastroesophageal reflux: gastric emptying study in a 7-year-old boy with nausea and vomiting showed delayed gastric emptying (**a**). Dynamic images revealed multiple episodes of gastroesophageal reflux (**b**), some of them reached to the upper esophagus, and it lasts for 20 s (only the first 12 min of dynamic images are shown here). Follow-up study after treatment with domperidone showed interval resolution of the gastric emptying (**c**)

Box 27.5 Protocol Summary for Meckel's Scan

Indications

Bleeding per rectum (painless or with pain) in a child, abdominal pain (in particular if there is questionable finding in other modalities such as ultrasound).

Contraindication

No pre-treatment with sodium perchlorate should be done. The study should be postponed at least 3–4 days after a barium study. The study should be postponed for at least 24–48 h for in vitro RBC scan. It is preferred to postpone the study longer (if possible) if DTPA, MDP, or a stannous agent was used (the stannous from these radiopharmaceuticals remains in the body for approximately 1–2 weeks, and when pertechnetate is administered, it binds to the stannous resulting in a label to RBCs).

Patient Preparation

NPO for 2–4 h.

Premedication with cimetidine (20 mg/kg p.o. for 2 days) or ranitidine (1 mg/kg, IV, 1 h before the study infused over 20 min) or glucagon (50 mg/kg IV over 10 min after the Tc99m pertechnetate

administration) with or without pentagastrin (6 mg/kg IV).

Radiopharmaceutical

^{99m}Tc-Pertechnetate: 1.85 MBq/kg (0.05 mCi/kg). Minimum dose of 9 MBq (0.25 mCi).

Effective dose (mSv/MBq): 0.013 [18].

Critical organ: proximal colon.

Image Acquisition

Dynamic imaging (with 128 word matrix, 60 s/frame) for 15 frames followed by static images (256 word matrix, 60 s per image, to include the following views: anterior, right lateral, and posterior abdomen) up to 60 min.

Processing and Analysis

Visual assessment. Pay attention to the other causes of a focal activity in the abdomen rather than heterotopic gastric mucosa and also causes of a false negative study (see text).

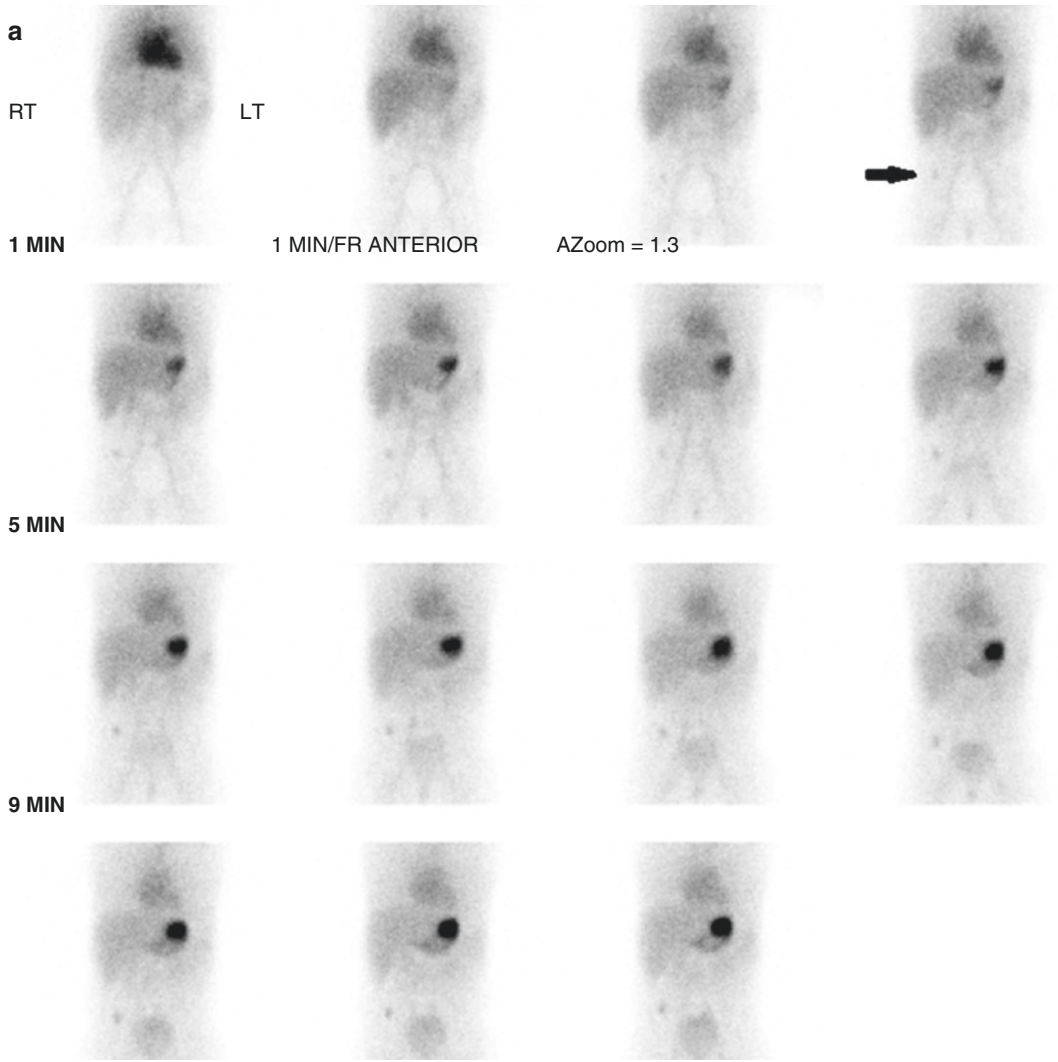

Fig. 27.6 Meckel's diverticulum containing heterotopic gastric mucosa: a small focal activity (arrow) was seen in the right lower quadrant at a rate similar to the gastric uptake (**a**). The activity was seen more lateral at 16 min (**b**) and moved close to the bladder at 30 min (**c**) image. The activity was clearly separated from the adjacent bladder on post-void image at 60 min (**d**)

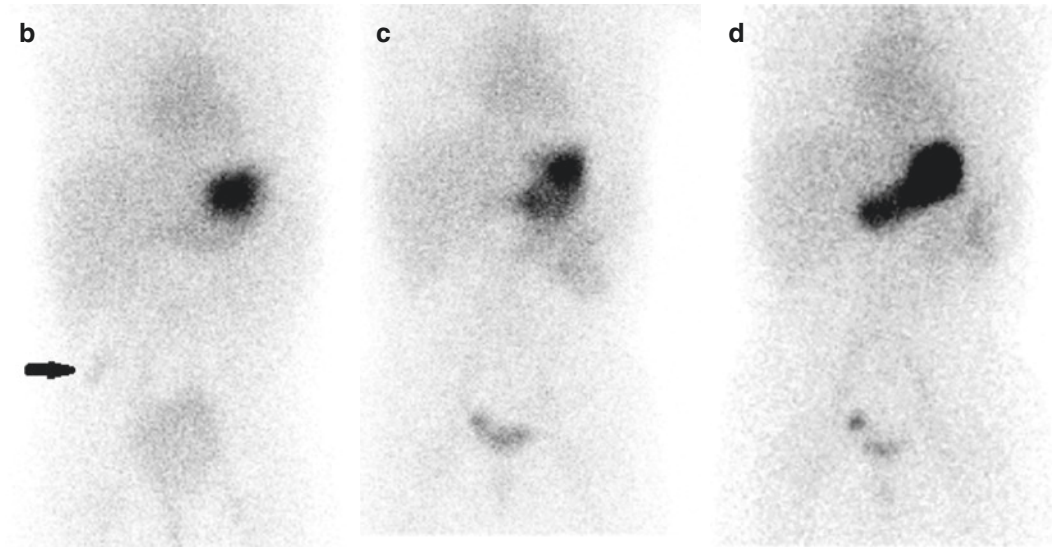

Fig. 27.6 (continued)

The sensitivity of the test can be increased by premedication options:

1. Histamine H2 blockers (cimetidine, ranitidine, famotidine) can increase the uptake of ^{99m}Tc-pertechnetate by inhibiting the release of the activity from the gastric mucosa. The dose is 20 mg/kg p.o. for 2 days for cimetidine or 1 mg/kg, IV, 1 h before the study infused over 20 min for ranitidine.
2. Pentagastrin, with a dose of 6 mg/kg IV, increases the duration and intensity of the ^{99m}Tc-pertechnetate uptake in the gastric mucosa. However, pentagastrin may increase intestinal motility and increase the activity washout.
3. Glucagon, with a dose of 50 mg/kg IV 10 min after the ^{99m}Tc-pertechnetate administration, can be used with pentagastrin or alone to reduce bowel motility.

If the patient is in emergency situation, there is no need for premedication. After the IV injection of 1.85 MBq/kg (0.05 mCi/kg) of ^{99m}Tc-pertechnetate (minimum dose of 9 MBq or 0.25 mCi), dynamic imaging (with 128 matrix, 60 s/frame) is obtained for 15 frames followed by static images (256 matrix, 60 s per image), to include the following views: anterior, right lateral, and posterior abdomen up to 60 min (Box 27.5).

A focal activity in the right lower quadrant, increasing over the time at a rate similar to the gastric uptake, is suggestive of a Meckel's diverticulum containing heterotopic gastric mucosa. However, other possibilities may mimic this pattern including vascular malformations, contamination, ulcers, hypervascular tumors, ectopic gastric mucosa other than Meckel's diverticulum (duplication cysts, Barrett's esophagus), ectopic kidney, accessory spleen, inflammation due to intestinal obstruction, intussusception, irritation due to consumption of certain drugs (ethosuximide or laxatives), and various urinary tract abnormalities such as dilated pelvis or ureters, extrarenal pelvis, hydronephrosis, bladder diverticulum, vesicoureteral reflux, obstruction, or vesicoureteral reflux.

In certain cases, the study may not show the heterotopic gastric mucosa in a Meckel's scan. These include insufficient gastric mucosa, washout of the secreted ^{99m}Tc-pertechnetate, dilution of radioactivity in small bowel due to hemorrhage, fast washout due to increased bowel movement, and impaired vascular supply due to intussusception, obstruction, or pressure from the adjacent organs (dilated ureter, bladder, or bowel). Poor techniques (inadequate preparation, no fasting, no premedication prior administration of potassium perchlorate, previous barium study, inadequate timing of imaging, and lack of

appropriate lateral and post-void images) are other important considerations for a false negative study [19].

27.10 Hepatobiliary Scan

Various indications are available for hepatobiliary scintigraphy including suspected cases of biliary atresia, choledochal cyst, cholecystitis, and biliary leakage. ^{99m}Tc-disofenin (2,6-diisopropylacetanilido iminodiacetic acid) and ^{99m}Tc-mebrofenin (bromo-2,4,6-trimethylacetanilido iminodiacetic acid) are usually used for hepatobiliary scintigraphy. ^{99m}Tc-mebrofenin (0.05 mCi/kg or 1.85 MBq/kg) is the preferred radiotracer to differentiate obstructive biliary tract diseases, such as biliary atresia from hepatocellular disorders (Box 27.6). The patient doesn't need to be NPO. Pre-treatment with phenobarbital (5 mg/kg/day divided bid for 3–5 days) or ursodeoxycholic acid (20 mg/kg/day in two divided doses for 2–3 days) prior to scintigraphy increases the test accuracy. The sensitivity and specificity of the test for biliary atresia are about 97% and 82%, respectively [10].

Box 27.6 Protocol Summary for Hepatobiliary Scan in Biliary Atresia

Indications

In suspected cases of biliary atresia (conjugated hyperbilirubinemia in early infancy).

Contraindication

Hypersensitivity to a hepatobiliary compound.

Patient Preparation

The patient doesn't need to be NPO (for non-biliary atresia scan, the patient should fast for 2–4 h).

Pre-treatment with phenobarbital (5 mg/kg/day divided bid for 3–5 days) or ursodeoxycholic acid (20 mg/kg/day in two divided doses for 2–3 days) prior to scintigraphy.

Radiopharmaceutical

^{99m}Tc-disofenin or ^{99m}Tc-mebrofenin 1.8 MBq/kg (0.05 mCi/kg), with a minimum administered activity of 18.5 MBq (0.5 mCi).

Effective dose: 1–2 mSv.

Critical organ: colon.

Image Acquisition

Dynamic anterior images (128 matrix, 60 s per frame using appropriate zoom setting) for 30 min followed by static images (256 matrix for 2 min each) in anterior and right lateral views at 1 h.

If no bowel activity is seen after 1 h of imaging, delayed static images (2, 4, 6, and 24 h) up to 24 h are acquired to detect any radiotracer excretion into the bowel.

Processing and Analysis

Visual assessment. Visualization of bowel activity excludes biliary atresia.

Immediately following injection of the radiotracer, dynamic abdominal images (128 matrix, 60 s per frame for 30 min using appropriate zoom setting) are acquired in anterior projection. At 1 h after injection, static (256 matrix for 2 min each, anterior and right lateral views) images are obtained. If no bowel activity is seen after 1 h of imaging, delayed static images (2, 4, 6, and 24 h) up to 24 h are acquired to detect any radiotracer excretion into the bowel. Excretion into the bowel excludes the presence of biliary atresia (Fig. 27.7). If there is no bowel activity, the study is suggestive of biliary atresia (Fig. 27.8). However, this pattern may be seen in severe cases of hepatocellular disease, sepsis, dehydration, TPN cholestasis, and bile plug syndrome in cystic fibrosis [11]. Thus, in practice, the value of hepatobiliary scan is to exclude biliary atresia (in case of visualization of bowel activity), not to diagnose it.

In children, acute cholecystitis may be due to gallbladder obstruction, or may be acalculous, secondary to sepsis, prolonged illness, vasculitis, or infections. Similar to the adults, non-visualization of the gallbladder is suggestive of acute cholecystitis. However, there is still

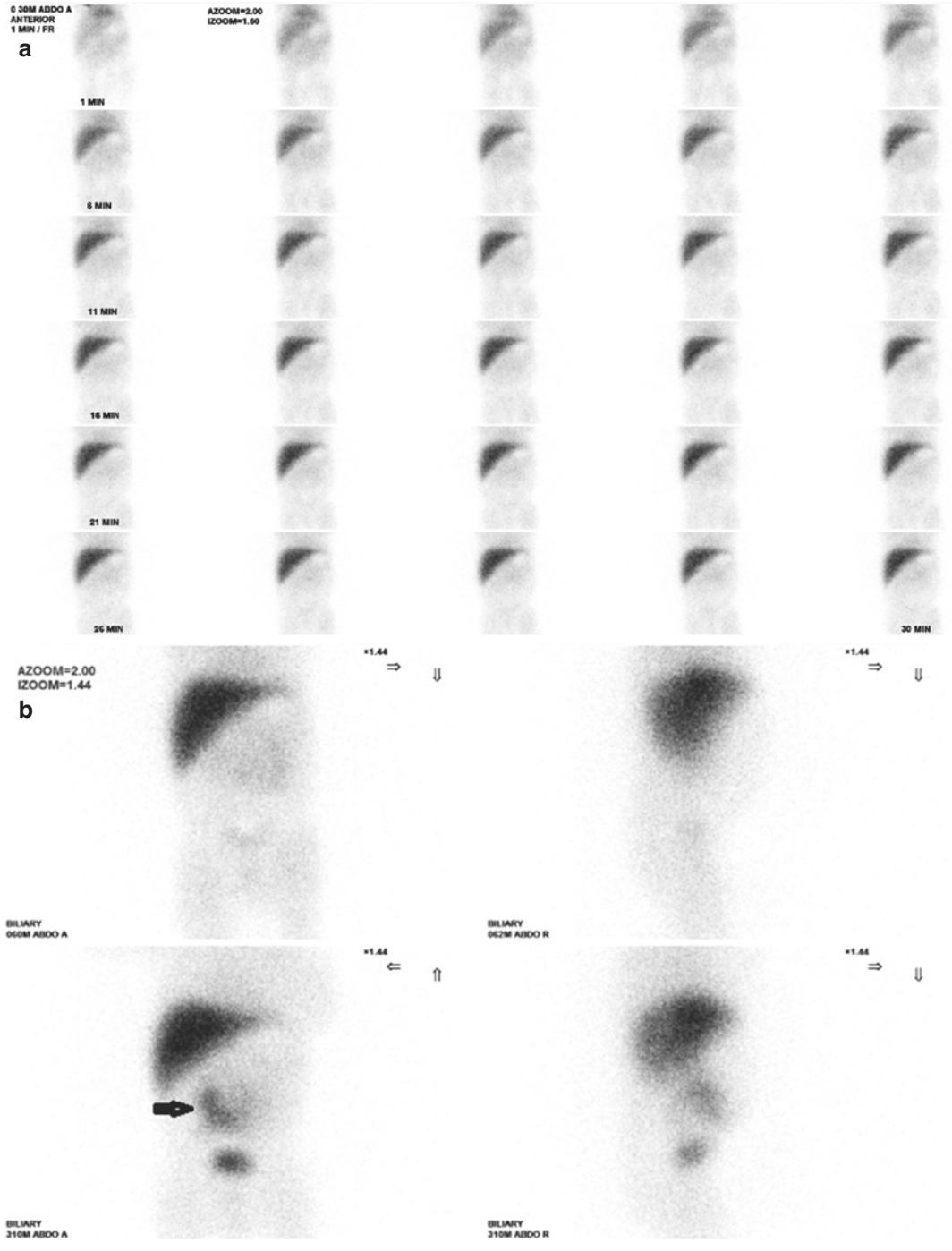

Fig. 27.7 No evidence of biliary atresia: hepatobiliary scan in a 4-week-old boy with conjugated hyperbilirubinemia showed good hepatic uptake with no drainage of activity into the bowel in the first 30 min (**a**). Bowel activity (arrow) was visualized on delayed images (4–6 h) which excluded the diagnosis of biliary atresia (**b**)

possibility of acalculous cholecystitis. If the gallbladder is visualized, response to a fatty meal or infusion of sincalide (0.02 mg/kg) is helpful to assess the contraction of the gallbladder. Hepatobiliary scintigraphy is also helpful to evaluate a biliary leak secondary to trauma or surgery.

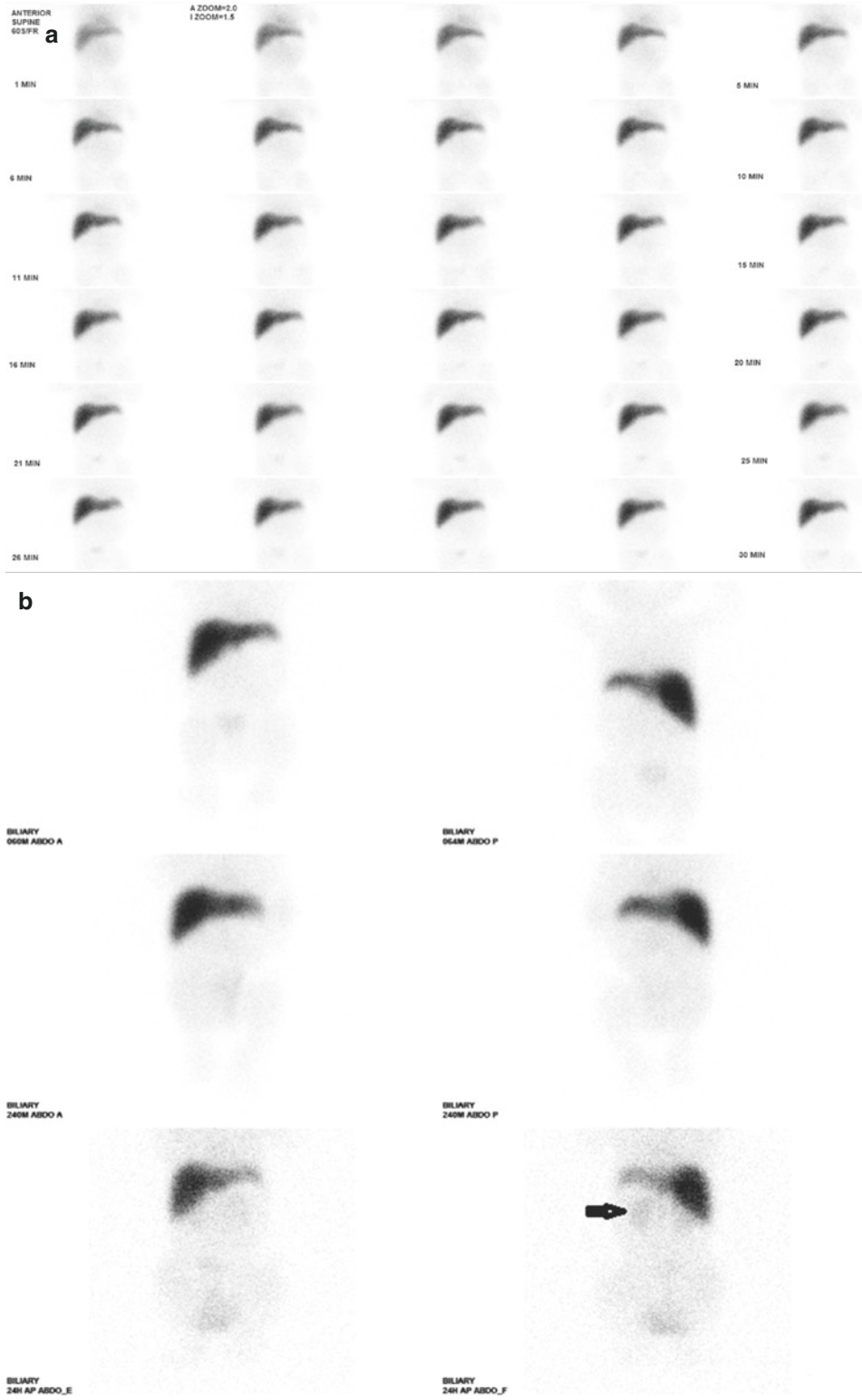

Fig. 27.8 Biliary atresia: hepatobiliary scan in a 5-week-old boy with conjugated hyperbilirubinemia showed good hepatic uptake with no drainage of activity into the bowel on early images (**a**) and delayed views (**b**) up to 24 h. Note the renal activity (arrow) seen in the abdomen on delayed images which is more prominent on posterior view

A biliary leak may be suspected by visualization of a fluid collection on US or CT scan. A hepatobiliary scan is a sensitive and noninvasive method that is able to establish an active hepatobiliary component associated with the fluid collection.

younger or small children, multiple static images can be acquired to avoid longer immobilization periods and thus minimize motion artifacts. In addition, this technique allows for better positioning of extremities [24].

27.11 Bone Scintigraphy

Bone scintigraphy is a very sensitive modality to evaluate benign and neoplastic bone diseases in both adults and children. ^{99m}Tc-Methylene diphosphonate (^{99m}Tc-MDP) is the most commonly used radiopharmaceutical for bone scintigraphy. This tracer concentrates in the amorphous calcium phosphate and crystalline hydroxyapatite reflecting both blood flow and osteoblastic reaction of bone. In accordance with the North American Consensus Guidelines, the recommended dose is 9.3 MBq/kg (0.25 mCi/kg) for children with a minimum dose of 37 MBq (1.0 mCi) [20]. The most recent version of EANM Paediatric Dose Card can also be used for optimal administered activities [21].

PET imaging using ^{18}F-NaF is being explored as an alternative method to bone scintigraphy with ^{99m}Tc-MDP. PET scanners have a greater ability than gamma cameras to image the high-energy photons of ^{18}F-NaF with similar radiation dosimetry and offer better sensitivity by improving spatial resolution [22, 23]. In addition, scanning can be acquired as early as 30 min after injection comparing with bone scintigraphy (using ^{99m}Tc-MDP), which requires imaging to be done 2–4 h after injection. This reduced time allows for faster and increased patient scheduling which can be beneficial for a busy nuclear medicine department.

Bone scintigraphy may include blood flow, blood pool, and delayed imaging and is known as three-phase imaging. Osteomyelitis is one of the most common indications for acquiring a three-phase bone scan in children. A blood flow study is obtained immediately after intravenous radiotracer injection for 1 min followed by blood pool images. Skeletal phase or delayed images are performed 2–4 h later (Box 27.7). Whole-body images are highly recommended in children regardless of the location of symptoms. For

Box 27.7 Protocol Summary for Bone Scintigraphy

Indications

Evaluate benign and neoplastic bone diseases.

Contraindication

Previously administered radiopharmaceutical (within 24–48 h).

Patient Preparation

No special requirements.

A topical anesthetic such as Maxilene can be applied prior to intravenous injection if needed.

Have patient void prior to imaging the pelvis or check if a diaper change is needed.

Radiopharmaceutical

^{99m}Tc-MDP: 9.3 MBq/kg (0.25 mCi/kg). Minimum 37 MBq (1 mCi) [44].

Effective dose: 2.7 mSv [1].

Critical organ: urinary bladder.

Image Acquisition

- **Flow Phase**: Dynamic images (1–3 s per frame) for 60 s.
- **Blood Pool Phase**: Immediate static images. 128 × 128 or greater matrix.
- 3–5 min/image or approximately 300,000 counts/image.
- **Skeletal Phase**: 2–3 h after tracer injection.
- Low-energy, high-resolution collimator is commonly used.
- Whole-body scan with speed 8–12 cm/min. 256 × 1024 matrix or greater.
- Spot views with 5 min/view or 300–500k counts/view. 128 or 256 matrix.
- **SPECT**: 60–64 images (20 s/view), 128 matrix or greater; zoom as required.
- **SPECT/CT**: CT acquisition should be strictly limited to the body segment of interest.

- CT settings should be individually adjusted according to the age and BMI.
- **Pinhole Collimator**: With 2 or 5 mm insert. Approximately 75k–100k counts/view.
- Dynamic acquisition could be used for motion correction to create a composite image.

Magnification technique with pinhole collimation improves resolution and can be particularly helpful in imaging small bony structures such as the femoral capital epiphysis. SPECT (single-photon emission computed tomography) can improve the sensitivity and specificity of planar images while providing better anatomic localization. Generally, SPECT studies are superior to planar images and are particularly useful in the evaluation of back pain [23, 25]. Combining the functional imaging of SPECT with the anatomic imaging of CT can further improve diagnostic accuracy and localization. SPECT/CT imaging systems are readily available and rapidly emerging as an important diagnostic tool in pediatric musculoskeletal imaging. In adult patients, SPECT/CT may be used for localization of osteomyelitis, inflammation, and both benign and malignant bone disease. Potential applications in children may include back pain and evaluation for suspected spondylolysis or enthesitis in the spinous processes [26, 27].

In order to appropriately interpret pediatric bone scintigraphy images, it is essential to know the unique normal physiologic distribution as well as pathologic findings in children. The normal distribution in pediatric bone scans may differ from adults. In children, high physeal and apophyseal uptake due to rich blood supply and active enchondral ossification is often noted. Absence of uptake in nonossified cartilaginous structures should not be mistaken for avascular necrosis. Regions where this may be of concern in younger children include the femoral capital epiphysis, patella, and navicular bone. Before ossification, the ischiopubic synchondrosis appears as a discontinuity of the inferior pubic ramus. During ossification, increased uptake in ischiopubic synchondroses is a common normal variant and should not be misinterpreted as a pathologic lesion [28].

Acute osteomyelitis is a common pediatric disease that can occur at any age, most often affecting children less than 5 years. Usually, it is the result of hematogenous spread of infection due to the rich vascular supply of the growing skeleton. It can be seen following direct puncture or spread of infection from contiguous structure [29]. Circulating organisms tend to infect the metaphyseal ends of the long bones (i.e., femur, tibia, and humerus), especially in the lower extremities, because of the high vascularity of the metaphyseal capillaries. In children less than 18 months, the presence of transphyseal vessels extending between the metaphysis and the epiphysis makes them particularly prone to septic arthritis of the adjacent joint. In older children, the growth plate is a relative barrier to the spread of infection into the epiphysis. Osteomyelitis in flat bones such as ilium and vertebrae is less frequent than in long bones [30]. Limping or refusal to bear weight is often the only symptom in older children. Radiography may be normal or only show deep soft tissue swelling within 48 h of infection. Three-phase bone scintigraphy is highly sensitive for the detection of osteomyelitis. Typically, a bone scan becomes positive 24–72 h after the onset of infection. The sensitivity of three-phase bone scan has been estimated as 94% with a specificity of 95% [31]. Ideally, the bone scan should be obtained before joint aspiration. However, diagnostic aspiration and antibiotic therapy should not be delayed until the bone scan is completed, as fine needle aspiration does not alter bone scan findings, nor does antibiotic therapy lead to a rapid change in bone scan [30]. A delayed whole-body scan on skeletal phase should be routinely obtained as osteomyelitis in children can be multifocal or present with referred pain. In addition, malignant disease such as leukemia and sarcoma may mimic acute osteomyelitis [25]. Blood flow, blood pool, and delayed images show focally high uptake in the affected bone. Occasionally, the affected bone in children shows low uptake [32]. This is most

likely due to reduced tracer delivery by increased intraosseous pressure from inflammation, edema, and joint effusion. Cellulitis can be differentiated from osteomyelitis as it typically demonstrates diffuse increased activity in the soft tissues on the dynamic and blood pool images, without focal osseous abnormality on delayed images.

Septic arthritis is more common in children younger than 3 years old with the hip and knee joints being the most commonly involved areas. Clinical findings include fever, pain, swelling, and erythema of the involved joint. Pain with passive motion is the most consistent finding in septic arthritis. Transient synovitis is the most common condition that mimics septic arthritis and is commonly seen in children less than 10 years old. It is typically preceded by a viral upper respiratory infection. Transient synovitis is a self-limited condition that most commonly involves the juvenile hip. It may be clinically indistinguishable from septic arthritis, and joint aspiration is often required. Early radiography may demonstrate the presence of a joint effusion with joint space widening and subluxation. Ultrasound can help in the detection of joint effusion. Echogenic material within the effusion suggests septic arthritis. In transient synovitis, the three-phase bone scan may be normal or can demonstrate diffuse increased flow and blood pool activity. Delayed images may demonstrate periarticular increased activity in the affected joint. If a bone scan is performed before joint aspiration, decreased tracer uptake on delayed images may be seen as a result of vascular compression by the joint effusion. The proper course of action is to aspirate the joint promptly. Generally, a bone scan is obtained after aspiration to detect any associated osteomyelitis [25].

Chronic recurrent multifocal osteomyelitis (CRMO) occurs most frequently in the latter half of the first decade and the first half of the second decade of life. Girls are more affected than boys. The clinical spectrum is often nonspecific with an insidious onset of localized warmth, tenderness, pain, and swelling. New sites of involvement can present as old sites resolve or are in various phases of healing. The disorder typically has a benign, self-limited clinical course with periodic exacerbations and remissions. Bone biopsy demonstrates fibrosis and inflammatory cells, but bone and blood cultures are negative. The metaphysis is the most common location of CRMO (Fig. 27.9). The most common anatomical sites are the long bones, spine, pelvis, and clavicles. Bone scintigraphy is helpful in identifying the multifocal bone lesions and typically demonstrates high uptake in both symptomatic and asymptomatic lesions [30, 33].

Legg–Calvé–Perthes disease is idiopathic ischemic necrosis of the femoral head in children. This disorder is most commonly seen in children between the ages of 5 and 8 years. Patients typically present with limping and pain in the affected hip. Bone scintigraphy is more sensitive than radiography for early diagnosis and is comparable to MRI [25]. In children, pinhole images can be obtained to improve the resolution. Generally, studies performed early after the onset of clinical symptoms show the absence of activity in the capital femoral epiphysis (Fig. 27.10) and can precede radiographic manifestations [34]. Later scans may demonstrate increased activity due to revascularization and remodeling.

Skeletal trauma can be evaluated by radiography. However, some injuries may be occult, and bone scintigraphy can help localize the abnormality and assist in diagnosis. Bone scintigraphy is highly sensitive and becomes abnormal as early as a few hours after injury. A toddler's fracture is a spiral or oblique fracture that most commonly involves the tibiae. Radiographic findings are often subtle and fractures may not be apparent. As such bone scintigraphy is a valuable tool for detecting this injury early before radiographic changes are present. Typically, the bone scan shows diffuse increased uptake in the tibial diaphysis (Fig. 27.11). A linear or spiral pattern of high uptake may be seen in some children [30].

Stress injury occurs due to repetitive stress on normal bone causing internal remodeling involving osteoclastic resorption and osteoblastic repair. Stress fractures can occur when resorption exceeds bone replacement which temporarily weakens the cortex [35]. Bone scintigraphy is

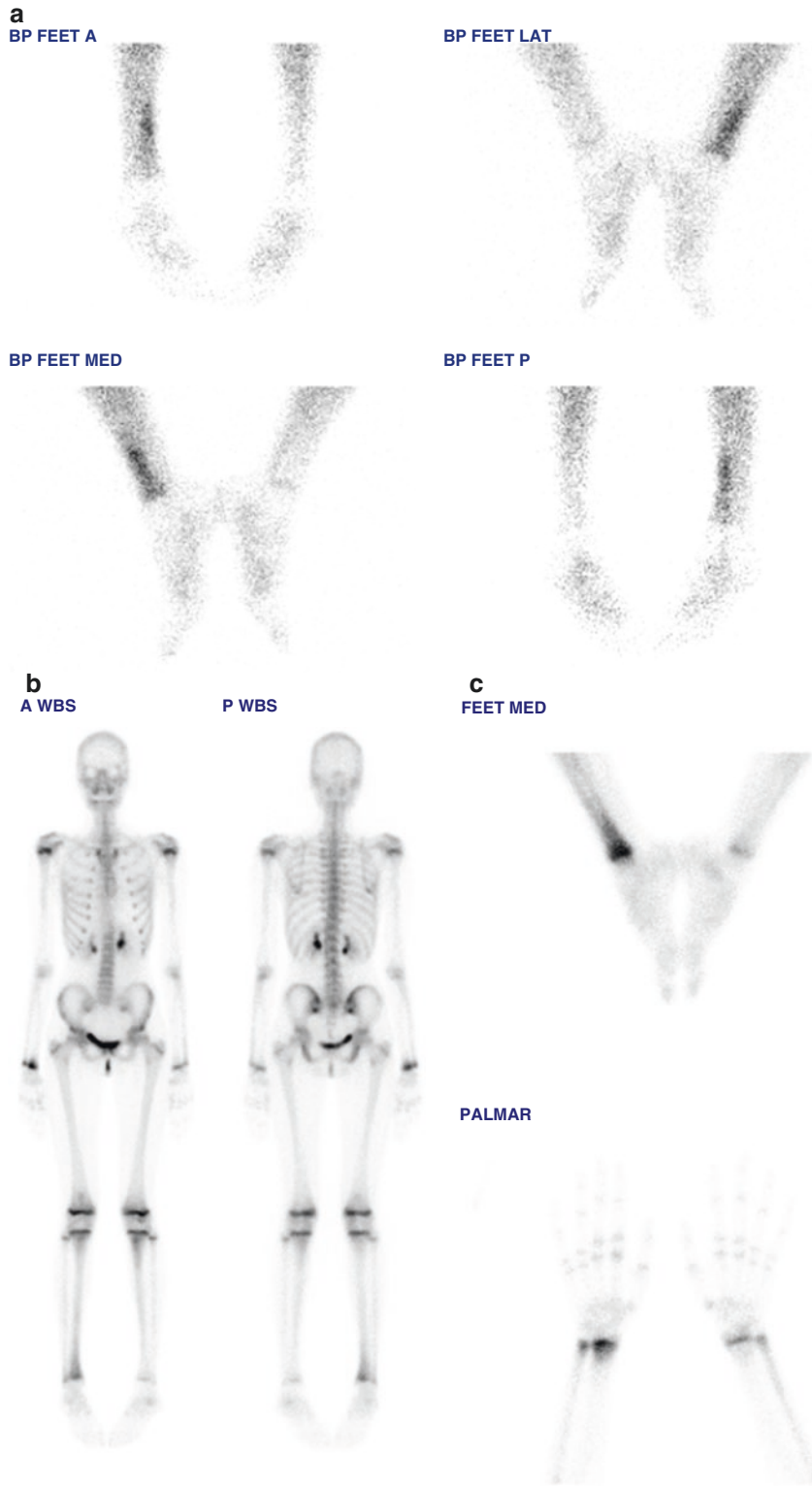

Fig. 27.9 CRMO: bone scan in a 15-year-old girl with CRMO presenting with right ankle swelling and redness. Blood pool images (**a**) showed asymmetric increased activity in the distal right tibia suggestive of hyperemia. On delayed whole-body scan (**b**) and spot views (**c**), there are multiple foci of increased activity in the distal right tibia, bilateral distal femurs, proximal left tibia, and distal right radius

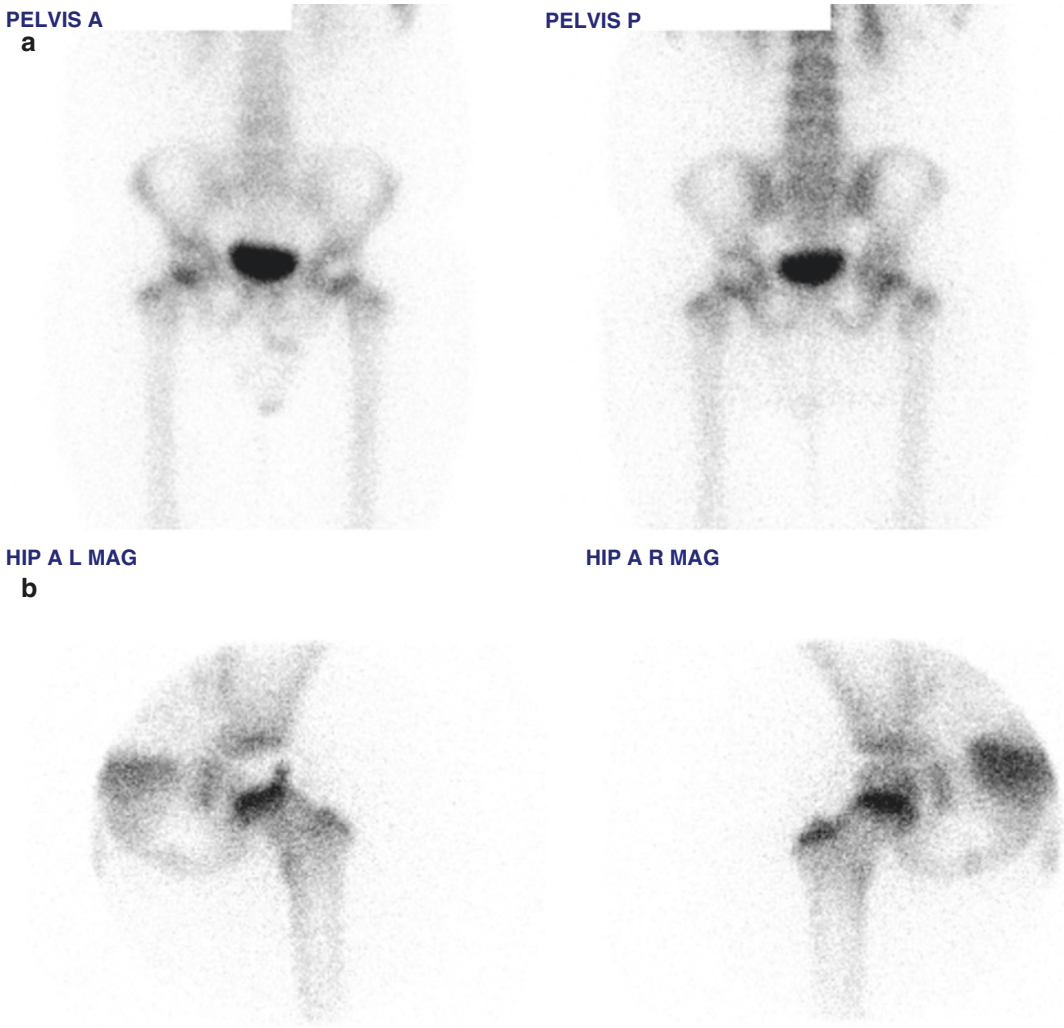

Fig. 27.10 Legg–Calvé–Perthes disease: planar (**a**) and pinhole (**b**) bone scan in a 6-year-old boy with limping shows decreased activity in the left femoral head suggestive of avascular necrosis

more sensitive than radiographs in detecting stress fractures. The bone scan is usually abnormal at the time of presentation and can precede plain film changes. MRI can be used in stress injury; however, unlike bone scintigraphy the entire skeleton cannot be easily screened on MRI.

Spondylolysis represents a stress fracture of the pars interarticularis of the vertebrae that occurs most commonly in the lower lumbar spine secondary to repetitive minor trauma such as hyperextension. However, congenital weakness of the pars as a result of hereditary factors also plays a role in its pathogenesis. Most patients present with either acute or chronic back pain. Sports such as gymnastics, diving, ballet, and contact sports such as football, hockey, and lacrosse are most commonly associated with spondylolysis. Bilateral spondylolysis may cause spondylolisthesis. Pars defects can be imaged with plain radiography, bone scintigraphy, computed tomography (CT), and magnetic resonance imaging (MRI). In bone scintigraphy, spondylolysis produces little or no abnormality on blood pool images. Delayed images typically show focally high uptake in the region of the pars interarticularis. SPECT imaging (or SPECT/CT) is more sensitive than planar studies and is recommended in evaluation of low back pain in young athletes [36]. Low back pain may arise from a lumbosacral transitional vertebral articulation

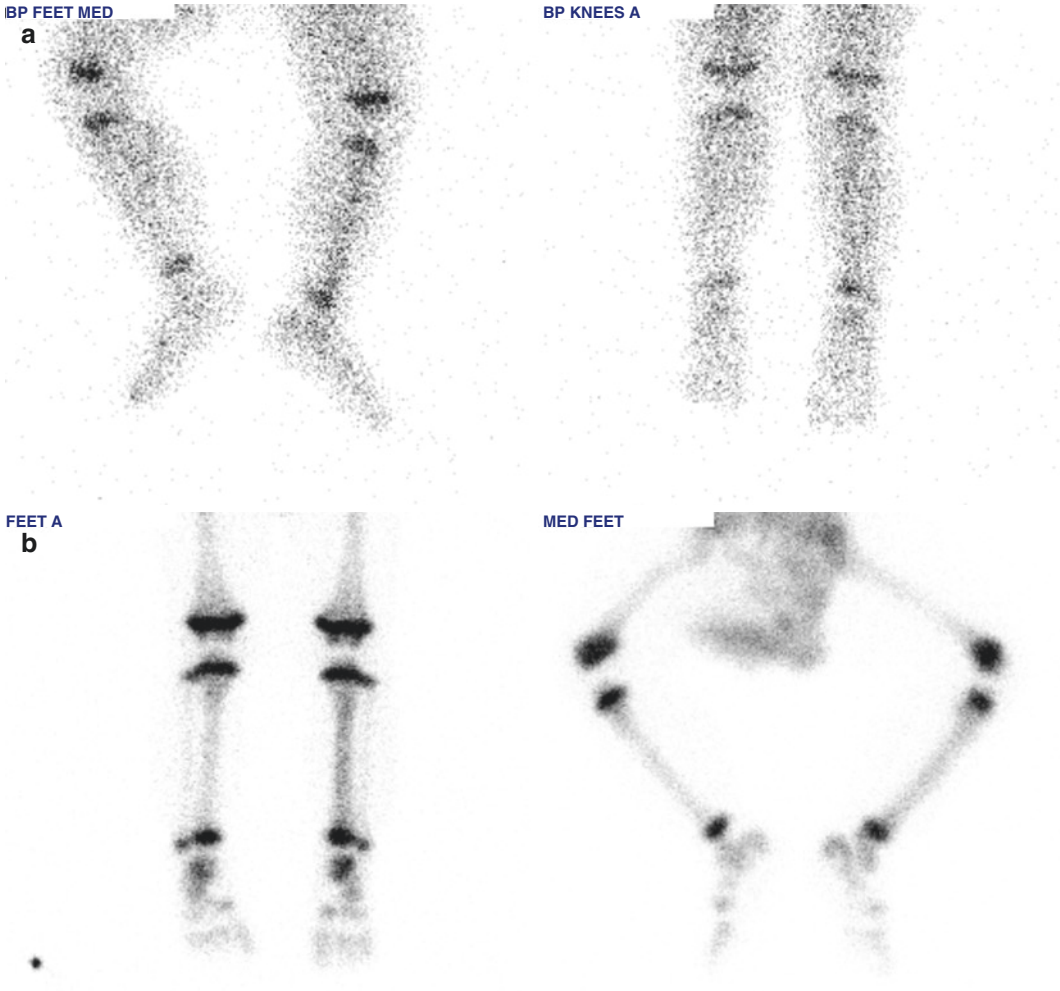

Fig. 27.11 Toddler's fracture: bone scan in an 18-month-old infant who fell down at daycare and was unable to bear his weight on the left side. Blood pool images (**a**) and delayed spot views (**b**) showed diffuse increased uptake in the left tibial diaphysis suggestive of toddler's fracture

which is a common congenital anomaly. Skeletal scintigraphy can show focally increased uptake along the transverse-sacral articulation of the transitional vertebra which supports the diagnosis of stress-associated injury with lumbosacral transitional vertebrae. As for spondylolysis, a SPECT study is superior to planar images (Fig. 27.12) and is recommended [23, 37].

In child abuse, bone scintigraphy is a complementary imaging modality to skeletal survey in diagnosis and management. Both modalities can be performed when child abuse is suspected [38]. Bone scintigraphy is useful when radiographs are normal, or detection of additional fractures would be helpful in confirming the diagnosis. It can provide a quick assessment to characterize the extent and severity of trauma and is more sensitive than radiographs for detection of rib fractures and nondisplaced diaphyses fractures of the extremities but is less sensitive for skull or symmetric metaphyseal fractures. Typically, rib fractures occur laterally, anteriorly, and posteriorly close to the costovertebral junction where the ribs are compressed against

Fig. 27.12 Spondylolysis: bone scan in a 14-year-old by with low back pain. Whole-body scan (**a**) didn't show any significant abnormality. SPECT study showed a focal increased activity in the left pars interarticularis visualized on coronal (**b**), axial (**c**), and sagittal (**d**) views

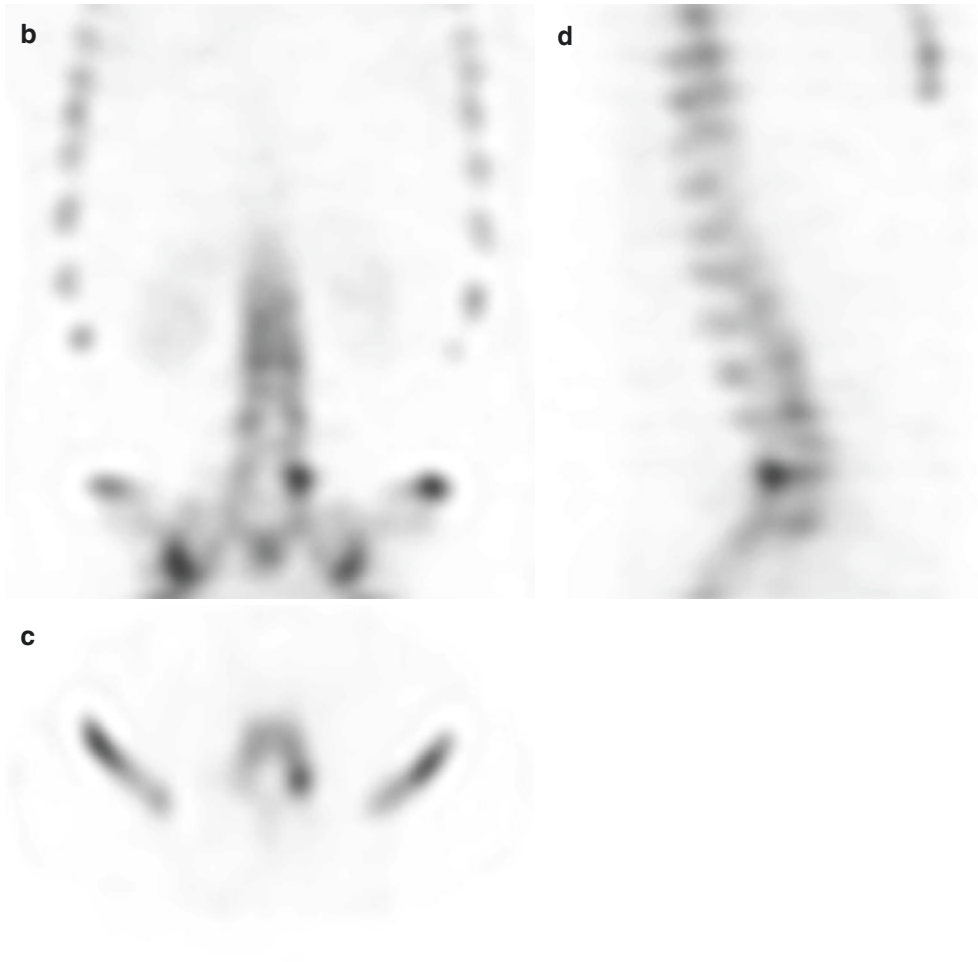

Fig. 27.12 (continued)

the transverse process [39]. ^{18}F-NaF PET has been evaluated for assessment of pediatric patients with suspected abuse. ^{18}F-NaF PET may have overall better sensitivity and is superior in the detection of rib fractures [40].

Reflex sympathetic dystrophy (RSD) or complex regional pain syndrome type I is a chronic pain syndrome. Trauma is the most common precipitating factor, which may be acute or remote by several months. RSD should be considered in a child who presents with persistent pain in the absence of laboratory and clinical findings. The typical findings on bone scan are hyperemia on blood flow and blood pool images with intense periarticular activity in the affected extremity. A cold variant of RSD has been reported in children characterized by decreased activity in the affected limb compared to the non-affected limb seen in the blood flow, blood pool, and delayed images [23].

Benign bone tumors are relatively common skeletal lesions in children and adolescents. Bone scintigraphy may play a role in localizing these lesions. Osteoid osteoma is a benign skeletal neoplasm of unknown etiology that is composed of highly vascular central nidus surrounded by reactive trabecular bone. The central nidus is usually smaller than 1.5 cm in diameter. The lesion can be cortical (most common), medullary, or periosteal. It can occur in any bone commonly in femur, tibia, and spine, but appendicular lesions are more common than vertebral lesions. Vertebral

lesions occur most often in the posterior elements and are frequently associated with a painful scoliosis. The most common location for a spinal lesion is the lumbar spine [36]. Osteoid osteomas occur most commonly in adolescents and young adults. The classic presentation is that of focal bone pain at the site of the tumor. The pain worsens at night and increases with activity. Bone scintigraphy is highly sensitive and usually shows increased activity in the flow and blood pool images. Delayed images demonstrate a focus of intense uptake in the nidus surrounded by diffuse and less intense uptake in the reactive bone [41]. Fibrous dysplasia is a development anomaly in which the normal medullary bone is replaced by fibrous tissue and can affect any bone. The monostotic form is more common and most frequently affects the ribs, femur, tibia, and craniofacial bones. The polyostotic form tends to occur in a unilateral distribution. However, bilateral involvement may occur with asymmetric involvement. The most common affected sites are the femur, tibia, and pelvis. Bone scintigraphy typically shows markedly increased uptake in both early blood pool and delayed images. At the initial presentation, bone scintigraphy is useful to demonstrate the extent of the disease [42].

Osteochondroma is the most common benign bone tumor and is defined as a cartilage-covered bony projection on the external surface of a bone. Most osteochondromas arise from tubular bones and are metaphyseal in location. It is found most commonly around the knee and the proximal humerus; however, it can occur in any bone. Bone scintigraphy shows varied accumulation of activity. Non-ossifying fibromas are well-circumscribed fibrous proliferations that occur most commonly in the juxta-epiphyseal regions of long bones. The most common site is the femur, followed by the tibia. The lesion is usually asymptomatic and discovered incidentally. The lesion usually regresses spontaneously. On bone scan, the lesion typically shows normal or mildly increased uptake. However, lesions that are ossifying may become quite active on bone scan during adolescence [43].

Osteosarcoma is the most common primary malignant bone tumor in children. The peak incidence is in adolescence and young adulthood. Children younger than 7 years are rarely affected. Osteosarcoma predominantly affects the metaphyseal regions of long bones. The most common locations for primary osteosarcoma are distal femur, proximal tibia, and proximal humerus. Flat bones are less frequently involved. Common sites for metastases are the lungs and bones. After radiography, initial imaging work up for osteosarcoma typically includes CT, MRI, and bone scintigraphy. CT of the chest is necessary to detect lung metastases. MRI of the primary lesion is used to assess the extent of intramedullary disease and surrounding soft tissue and to later distinguish postoperative changes from residual or recurrent disease. Bone scintigraphy typically is used to detect distant metastases or skip lesions and later to evaluate therapy response and recurrent disease. Primary tumors and skeletal metastases typically show marked uptake. Occasionally bone scintigraphy demonstrates pulmonary metastases due to osteoid production by the metastatic deposits. However, it is much less sensitive than CT in the detection of pulmonary metastases [25].

Ewing sarcoma is the second most common primary bone malignancy in children arising from mesenchymal origin. It often occurs in the second decade of life with peak age range from 4 to 15 years. Males are affected more than females. The most common presenting symptoms are pain and swelling. Although any bone can be affected typically, the bones of the pelvis, femur, tibia, spine, ribs, and humerus are involved with lungs and skeleton being the most common sites of metastases [30]. The diagnosis of Ewing sarcoma is usually made by radiographs which typically show an aggressive lytic lesion in the metaphysis or diaphysis of the bone, with a soft tissue mass extending from the bone. CT scanning helps to define the bone destruction that is associated with Ewing sarcoma. MRI can also be used to assess the extent of Ewing sarcoma. Whole-body bone scans can provide information about the primary lesion, presence of any skip lesions, or distant metastases during tumor staging. It is also recommended for end of treatment evaluation [23].

27.12 MIBG Scan

MIBG scans (labeled with I-131 or I-123 and recently I-124) have been used in neuroectodermal tumors including pheochromocytoma (Pheo) and neuroblastoma (NBL) for about 40 years. ^{123}I-MIBG is the preferred radiotracer in children due to lower radiation dose and better image characteristics (shorter half-life, 13 h; ideal energy of γ-ray: 159 keV). Moreover, the study can be completed in a shorter period of time. Patient preparation is important for MIBG scan. The pre-treatment with sodium or potassium perchlorate (300–600 mg/m^2 BSA) daily (5 days before scanning for ^{131}I-MIBG or 1 day for ^{123}I-MIBG) or Lugol's iodine solution (0.3 mL) three times a day (3 days before for ^{131}I-MIBG or 1 day for ^{123}I-MIBG) to block the thyroid uptake is necessary (Box 27.8). These medications should be continued for 1–2 days for ^{123}I-MIBG, or 2–3 days for ^{131}I-MIBG after scanning [56]. A number of drugs may interfere with MIBG uptake and should be discontinued before the exam (please refer to EANM procedure guidelines for ^{131}I-MIBG therapy. Eur J Nucl Med Mol Imaging. 2008). Foods containing vanillin and catecholamine-like compounds (e.g., chocolate and blue-veined cheeses) may also interfere with MIBG uptake [56].

Box 27.8 Protocol Summary for MIBG Scan

Indications

For confirmation, staging, response to therapy, and evaluation of relapse in neuroectodermal tumors.

Contraindication

Contraindicated in patients medicated with certain agents; please refer to the EANM 2010 guideline for MIBG therapy [60].

Patient Preparation

Pre-treatment with sodium or potassium perchlorate (300–600 mg/m^2 BSA) daily (5 days before scanning for ^{131}I-MIBG or 1 day for ^{123}I-MIBG) or Lugol's iodine solution (0.3 mL) three times a day (3 days before for ^{131}I-MIBG or 1 day for ^{123}I-MIBG) to block the thyroid uptake.

These medications should be continued for 1–2 days for ^{123}I-MIBG or 2–3 days for ^{131}I-MIBG after scanning. Patient should be encouraged to drink water and void frequently.

Radiopharmaceutical

^{123}I-MIBG, 7.4 MBq/kg; minimum, 37 MBq, maximum, 400 MBq.

Effective dose (mSv): 3.7 [1].

Critical organ: urinary bladder [58] and liver [56].

Image Acquisition

Whole-body scan (scan speed 5 cm/s, matrix of 256 × 1024, in supine position) or spot views (5–10 min/view, 256 matrix, and zoom as required) with either a low-energy high-resolution (LEHR) or a medium-energy high-resolution (MEHR) collimator (20% energy window centered at 159 keV).

SPECT consists of 120 projections, in steps of 3° (in continuous or step and shoot mode), 25–35 s per step (matrix 128). In noncooperative patients, the acquisition time can be reduced using steps of 6° or a 64 × 64 matrix [60].

Processing and Analysis

The processing parameters depend on the camera. Iterative reconstruction with a low-pass post-filter often provides better images than filtered back projection [60].

Visual interpretation. Any focal activity other than physiologic MIBG uptake is considered suspicious. Semiquantitative evaluation (e.g., Curie score) can also be recorded.

The radiotracer should be infused slowly (over 5 min) with a dose of 0.52 MBq/kg (3.7–18.5 MBq) for ^{131}I-MIBG and 7.4 MBq/kg (37–400 MBq) for ^{123}I-MIBG. The recommended minimum and maximum doses are 37 MBq and

400 MBq for ^{123}I-MIBG and 3.7 MBq and 18.5 MBq for ^{131}I-MIBG, respectively [57]. Imaging is acquired at 24, 48, and 72–96 h (for ^{131}I-MIBG), or at 24 and 48 h (for ^{123}I-MIBG) after radiotracer administration (please see Box 27.8 for the technique of acquisition). SPECT views from the chest, abdomen, and pelvis are usually obtained with ^{123}I-MIBG scan.

The uptake of MIBG is varied in different types of neuroectodermal tumors; it is not possible to differentiate different types of neuroectodermal tumors based on the positivity and intensity of MIBG uptake [59]. However, neuroblastoma (NBL) usually shows a good uptake of MIBG. NBL is the most common extracranial solid tumor in children frequently seen during infancy. The clinical behavior and prognosis of NBL are variable in different patients and different age groups; some may regress spontaneously even without treatment, and some may progress and metastasize rapidly with poor prognosis despite aggressive therapy. One of the tools to evaluate patient prognosis is staging based on the International Neuroblastoma Staging System (INSS). The classification evaluates the disease distribution using radiographic and scintigraphic studies, surgical operability, and lymph node and bone marrow involvement. As metastases are relatively common at presentation, accurate staging depends on multimodality imaging. An MIBG scan is a sensitive (approximately 90%) and very specific (approximately 95–100%) modality for the detection of NBL (Fig. 27.13) [57, 59]. However, in up to 10% of NBL, the tumor is not MIBG avid. MIBG-negative NBL tumors are a clinical challenge and are usually seen in stage I and II tumors [61]. As NBL cell lines may have somatostatin receptors, new radiotracers with DOTA-conjugated peptides (e.g., ^{68}Ga-DOTATATE, ^{68}Ga-DOTATOC) may have a role in NBL, in particular when a radionuclide therapy (e.g., ^{177}Lu-DOTATATE) is an option [62, 63]. If the tumor is MIBG avid at diagnosis, MIBG scan can be used for evaluation of response to treatment, prognosis, and follow-up surveillance and when the treatment regimen changes.

27.13 ^{18}F-FDG PET/CT

The clinical application of PET/CT in the management of pediatric malignancies has been shown in several studies during the last decade. In general, the clinical application and the technique are similar to adults including staging, response to therapy and evaluation of relapse in a variety of tumors, as well as selection of the best site for biopsy and for the evaluation of fever of unknown origin (FUO) [67, 74, 75]. There are, however, physiologic variations in FDG biodistribution and potential pitfalls in the pediatric population which merit special attention.

The palatine and lingual tonsils are very active during childhood. Moreover, clinical or subclinical upper respiratory infection is relatively common in children. Thus, it is not uncommon to see increased ^{18}F-FDG activity in these structures, even without apparent inflammation (Fig. 27.14a). The intensity of the activity and the symmetric/asymmetric pattern of activity and correlative CT findings may be helpful to differentiate a normal variant versus pathology. In a physiologic uptake, the activity is usually symmetric, and the intensity of the uptake is mild to moderate with no correlative CT findings.

The activity in the thymus is more prominent in pediatric population. The thymus often shows mild to moderate homogeneous increased activity with a quadrilateral shape during early childhood and a more triangular shape during adolescence (Fig. 27.14b). Thymus activity may also increase in thymus hyperplasia after chemotherapy, particularly in young patients with lymphoma or testicular cancer. An abnormality is suspected if the thymus activity is heterogeneous or focal, or the intensity is high, or there are any abnormal findings on the correlated CT. In a study by Sasaki et al., the average SUV for thymic carcinoma was much higher (7.2 ± 2.9) than invasive thymoma (3.8 ± 1.3) and noninvasive thymoma (3 ± 1) [77]. Ferdinand et al. suggested an SUV cutoff of 5 to differentiate thymic carcinoma from thymoma with a sensitivity of 84.6%, specificity of 92.3%, and accuracy of 88.5% [76].

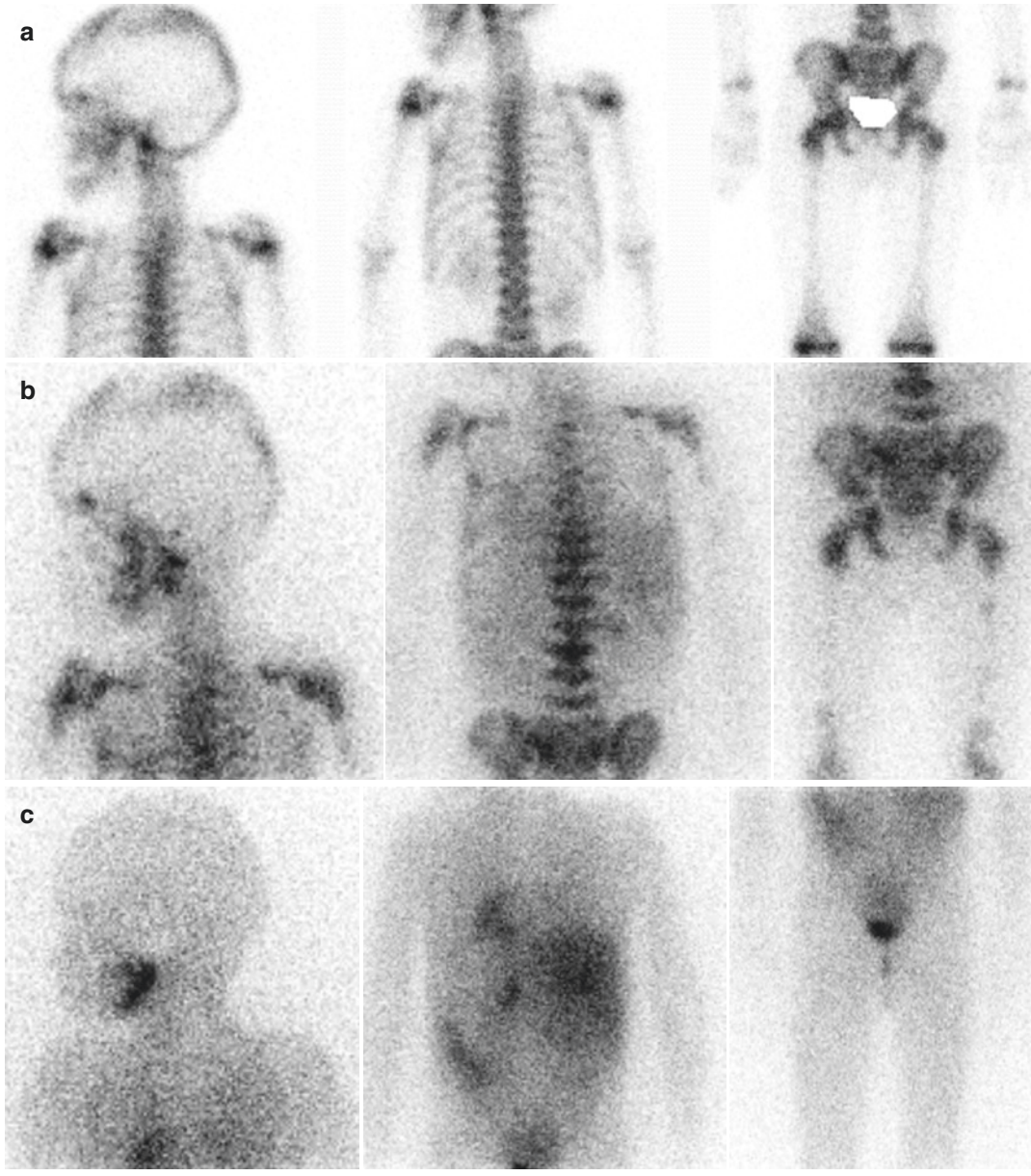

Fig. 27.13 Bone/bone marrow metastases on MIBG scan: bone scan in a 4-year-old boy with NBL showed an abnormal activity in the skull with no significant abnormal uptake in the vertebrae, pelvis, and femurs (**a**). ^{123}I-MIBG scan revealed multiple bone/bone marrow metastases (**b**). Complete resolution of the lesions was noted on a follow-up ^{123}I-MIBG scans 5 months after treatment (**c**)

Increased activity in the brown fat is more common in children than in adults. The brown fat uptake is usually seen in the neck region extending inferiorly in the upper shoulders, superior and posterior mediastinum, diaphragmatic hiatus, and suprarenal area (Fig. 27.14c). Brown fat uptake corresponds to hypodense regions on CT and should be differentiated from lymph nodes activity. Some medication such as propranolol and diazepam may reduce brown fat uptake. As there is an association between brown fat uptake and cold temperature, we control the room tem-

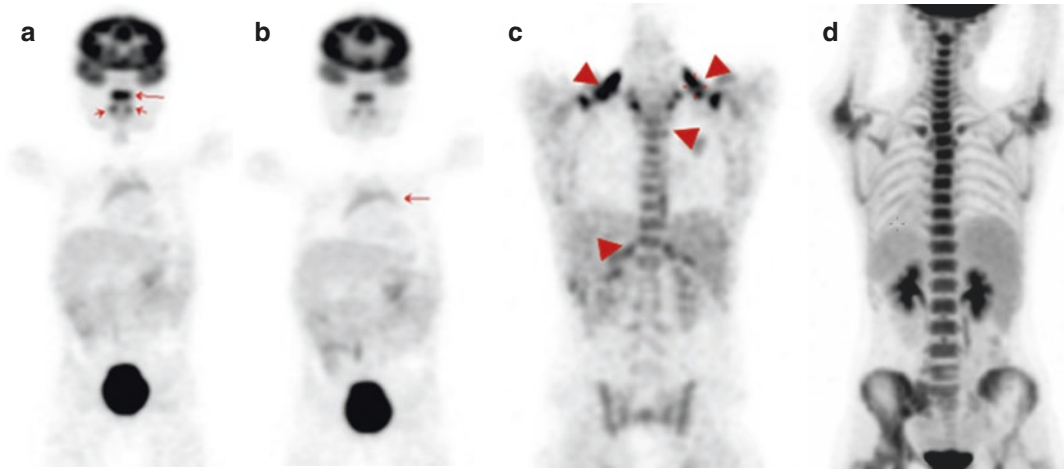

Fig. 27.14 FDG PET in children: physiologic increased activity in the tonsils (arrow) (**a**), thymic activity (arrow) (**b**), brown fat uptake (arrow head) (**c**), and increased bone marrow activity after G-CSF administration (**d**)

perature of the injection room in our hospital and often place a warm blanket over the patient during the uptake phase.

There are other special considerations that are useful for interpretation of PET/CT findings in children. Bone marrow activity is often more active in children than adults, likely due to greater red marrow component. Bone marrow uptake may be more prominent following a hematopoietic drug stimulators injection such as granulocyte colony-stimulating factor (G-CSF) (Fig. 27.14d). It is suggested to perform the PET study 2–3 weeks postinjection of G-CSF, if possible. Children may move a lot during the uptake phase. Therefore, it is not infrequent to see increased activity in a group of muscles. Patient movement during scanning may cause misregistration of PET and CT images and can create artifacts. Reviewing the non-attenuation corrected images is helpful for interpretation of these cases. Increased activity in the vocal cords or accessory respiratory muscles may be also seen due to the child's screaming or crying. The vocal cords uptake in these scenarios is usually symmetrical. In case of asymmetric vocal cord activity, correlation with CT scan is helpful to diagnose any possible pathology.

Finally, the standardized uptake value (SUV) of the lesions cannot be simply extrapolated from the adults' numbers. Additionally, the consistency of SUVs is more challenging in children as the body composition is changing over time. Fat has lower FDG uptake than other tissues. The percentage of fat to body weight is about 11% in newborn, rises to about 26% at 5 months, and then decreases gradually until 12 months of age [78]. This may affect the SUV consistency during infancy. The technique of PET/CT in children is varied in different centers depending on the camera information and institutional policy (Box 27.9).

Box 27.9 Protocol Summary for PET/CT Scan

Indications

For staging, response to therapy, and evaluation of relapse in different tumors; for selection of the best site for biopsy in malignancies; for evaluation of fever of unknown origin (FUO).

Contraindication

Nothing.

Patient Preparation

No heavy exercise for at least 48 h. NPO for 4 h (except for water).

Check the glucose level (should be <11 mmol/L or 200 mg/dL). For diabetic patients follow specific guidelines.

The patient should be relaxed and in a warm room during the uptake phase.

G-CSF should be stopped 2–3 weeks before the exam if possible.

Radiopharmaceutical

^{18}F-FDG: 5.2 MBq/kg; minimum, 37 MBq, maximum, 370 MBq.

Effective dose (mSv/MBq): 0.056 [79].

Critical organ: urinary bladder [79].

Image Acquisition

Imaging starts 60 min after radiotracer injection. Acquisition parameters and patient positioning will vary depending on the indication provided on the requisition and the PET/CT camera. In general, for lymphoma patients, with no evidence of bone involvement, imaging from basal skull to mid-thigh is adequate. For certain conditions such as sarcoma, Langerhans cell histiocytosis, neuroblastoma, and thyroid, whole-body acquisition (to include skull and extremities) is required.

PET acquisition time: 2–3 min/bed position.

CT can be done as a low-dose CT for attenuation correction or a diagnostic CT scan when it is needed.

Processing and Analysis

Filtered back projection or iterative reconstruction depending on the camera parameters.

Other PET tracers have also been used in children. The use of ^{18}F-fluoro-L-DOPA (^{18}F-DOPA) PET/CT in congenital hyperinsulinism (CHI) is a good example. The result of surgery in CHI has been improved recently, mainly because of the better delineation of the lesion using ^{18}F-DOPA PET/CT [64]. Congenital hyperinsulinism may be due to a focal area of secreting insulin cells, a diffuse form of lesions, and atypical forms of scattered segmental mosaic lesions. In focal CHI, or a segmental mosaic form, surgical resection is the main treatment. However, it is important to resect enough tissues to minimize relapse and to avoid too much resection in order not to induce diabetes. This is especially important in the segmental mosaic form. In diffuse CHI, however, there is a recent tendency toward medical therapy due to high frequency of relapse or surgical induced diabetes [66]. There is also a possibility of spontaneous improvement of hyperinsulinemic hypoglycemia (perhaps because of apoptosis) in diffuse CHI [64].

As the focal lesions are mainly an accumulation of diseased islet cells secreting insulin without control (but not a tumor), it is very hard to be distinguished during surgery even with magnifying lenses [65]. ^{18}F-DOPA PET/CT is very useful to guide the surgeon for appropriate surgical resection of focal and segmental mosaic forms during the surgery. PET/CT is also useful to select the appropriate technique of surgery. For example, if PET-CT shows a lesion in the pancreatic tail, primary laparoscopic resection is probably a better approach.

27.14 PET/MR

Combined PET/MRI has been recently used as important clinical and research tools. There are many clinical indications for PET/MR in children including staging, response to therapy (e.g., lymphoma, sarcoma, neuroblastoma, and neurofibromatosis type 1), and surveillance of cancers and in neurology [68–71]. The main advantages of PET/MR to PET/CT are the low radiation and better delineation of soft tissue. Using MR instead of CT will reduce the radiation dose by about 50–80% [72, 73]. Attenuation correction is technically difficult with MR. However, there are some improvements in terms of measurement of SUV using a specific technique called segmentation-based attenuation correction [73].

27.15 Brain Scintigraphy for Brain Death

Brain death in neonates, infants, and children relies on a clinical diagnosis that is based on the absence of neurologic function with a known irreversible cause of coma. Coma and apnea must coexist to diagnose brain death. This diagnosis should be made by physicians who have evaluated the history and completed the neurologic

examinations [80, 81]. The diagnosis of brain death should not be made based on neurologic examination alone if high therapeutic levels of sedative agents have been administered. If uncertainty remains, an additional study such as brain scintigraphy should be performed, although this study is not a substitute for the neurologic examination.

Additional studies can be used to help in making the diagnosis of brain death to reduce the observation period, or when components of the examination or apnea testing cannot be completed safely, or if there is uncertainty about the results of the neurologic examination, or if a medication effect may interfere with evaluation of the patient. If the ancillary study supports the diagnosis, the second examination and apnea testing can then be performed [80]. In some countries other than the United States, a confirmatory test is required by law [82].

Conventional cerebral radionuclide angiography followed by planar scintigraphy with ^{99m}Tc-pertechnetate or ^{99m}Tc-diethylenetriaminepentaacetic acid (DTPA) can be used in children with an equivocal clinical diagnosis of brain death which is based on flow images followed by static planar images in anterior and lateral projections [83]. However, imaging with brain-specific tracers such as ^{99m}Tc-ECD or ^{99m}Tc-HMPAO has currently been used more frequently, allowing for better visualization of posterior fossa and brain stem perfusion [84]. Brain-specific radiotracers are preferred as interpretation is less dependent on the quality of the bolus and early dynamic images. These radiotracers provide an assessment of cerebral flow on the first pass flow images as well as on delayed planar and SPECT views [83]. The typical dose for children is 11.1 MBq/kg (0.3 mCi/kg) with a minimum dose of 185 MBq (5 mCi). Flow images are acquired at the time of tracer injection at 1 s per frame for 60 s. If better spatial resolution is required, images can be combined into 2 s per frame for display purposes. If nonspecific radiotracers are used, static planar images are acquired in anterior and lateral views and posterior if possible. Planar images should be acquired approximately 20 min after injection in addition to the flow images [83]. Single-photon emission computed tomography (SPECT) can be performed to provide a better visualization as it can be helpful for differentiating overlying scalp from intracranial activity and for evaluating the posterior fossa [85].

When nonspecific radiotracers are used, the lack of flow in dynamic flow study on anterior view, in combination with the absence of activity in the venous sinus on static images, suggests the diagnosis of brain death. However, faint activity of venous sinuses may be seen in children with nonspecific brain tracers, which makes it difficult to interpret. Coker et al. reported sinus activity in 14 of 55 children who had confirmed brain death [86].

Using specific agents such as ^{99m}TC-HMPAO, the planar or SPECT images should demonstrate no cerebral or cerebellar activity in addition to absent of brain flow (Fig. 27.15) [87]. Usually, this brain imaging study is not affected by drug intoxication or hypothermia (as the EEG may be) and is more specific for brain death. The sensitivity of planar imaging using ^{99m}Tc-HMPAO is very high, and the specificity is virtually 100%. To evaluate the reliability of SPECT imaging in the diagnosis of brain death, Facoo et al. evaluated 50 comatose patients with SPECT imaging using ^{99m}Tc-HMPAO. SPECT imaging confirmed the diagnosis of brain death in 45 out of 47 patients (95.7%). Activity in the basal ganglia, thalamus, or brain stem was noted in two clinically brain-dead infants [88]. In certain cases, the intracranial pressure may not increase significantly (due to open fontanels) in infants. Therefore, brain uptake may be present despite the clinical diagnosis of brain death. Ashwal et al. reported a brain uptake in 6 of 17 infants with clinical brain death; three of them were preterm infants [89]. The remaining 11 infants had no cerebral blood flow. Okuyaz et al. also reported two newborns needed a second image to confirm the diagnosis. In this study, eight patients who fulfilled the clinical criteria of brain death were evaluated using ^{99m}Tc-HMPAO SPECT, and six patients demonstrated lack of perfusion activity in the cerebrum in their first SPECT study [84]. Thus, a brain death study should be interpreted with caution especially in infants.

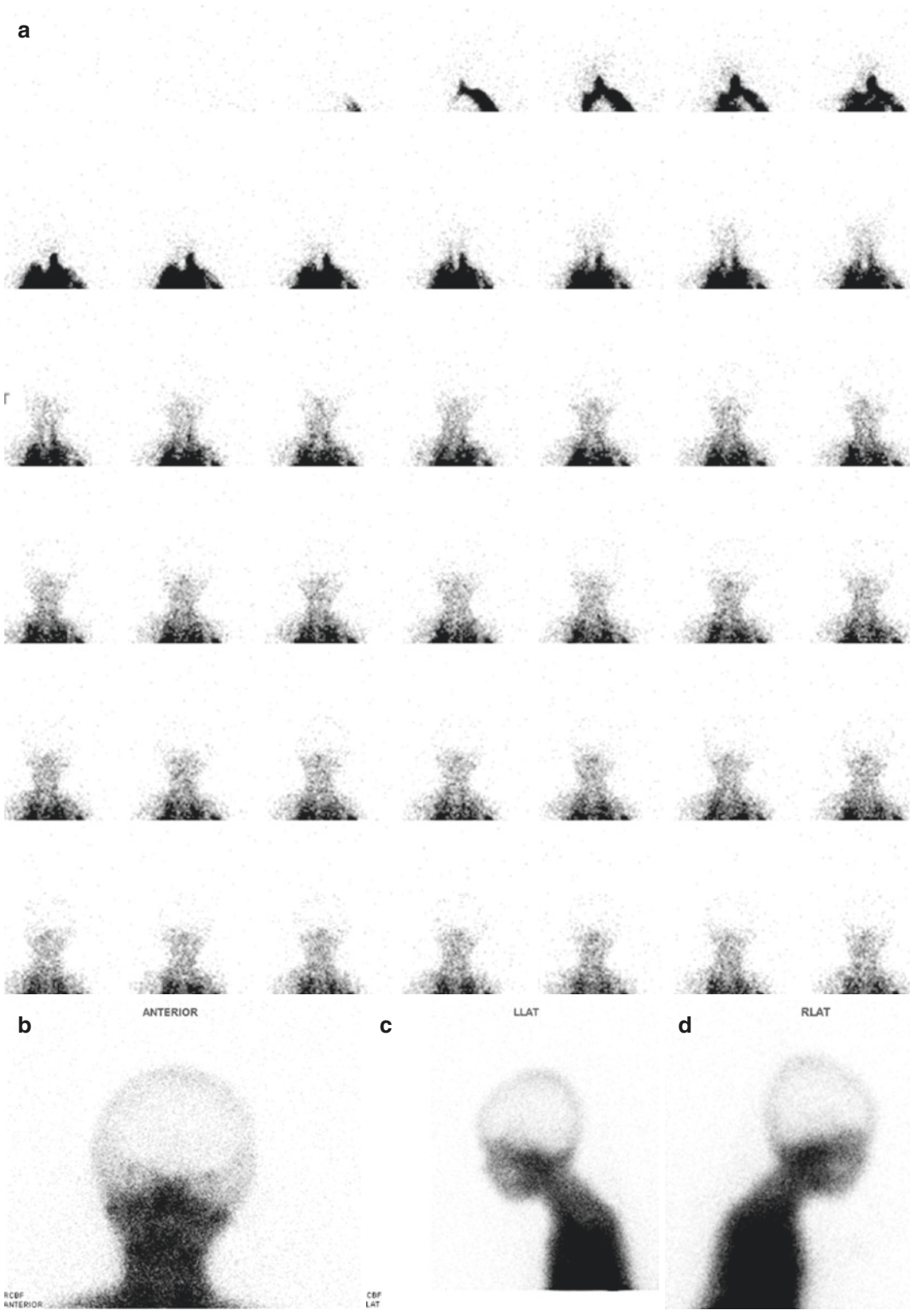

Fig. 27.15 Brain death: a 4-year-old boy with brain death after drowning. Early dynamic images (**a**) as well as delayed static views after 20 min in anterior (**b**) and lateral projections (**c**, **d**) didn't show any activity in the brain

27.16 Ventilation/Perfusion Scans for Pulmonary Embolism

Pulmonary embolism (PE) in the pediatric population is relatively less common than in adults. However, improvements in pediatric care have led to an increase in the survival of chronic or critically ill children and, thus, an increase in the risk and incidence of common complications encountered by such patients, including PE [45]. Buck et al. reviewed autopsies performed in children and found a PE incidence of 4%. They concluded that PE in children is underdiagnosed and using lung perfusion scintigraphy should be encouraged [46].

Cancer, immobility, central venous lines, vascular malformations, nephrotic syndrome, long-term total parenteral nutrition administration, systemic lupus erythematosus, ventriculoatrial shunts, congenital and/or acquired thrombotic tendencies, and acute DVT are all recognizable risk factors associated with PE in children [47].

The clinical findings of PE in children are similar to those encountered in adults. However, none of these signs and symptoms is specific to establish the diagnosis of PE and could be associated with underlying comorbid disease, reducing the level of suspicion by clinicians. The symptoms of PE in children may include shortness of breath, pleuritic chest pain, and hemoptysis. However, the clinical presentation may vary and may be subtle and mimic other diseases [45]. In adolescents, pleuritic chest pain is the most common presenting complaint, followed by dyspnea, cough, and hemoptysis [47]. Other signs and symptoms may include wheezing, rales, sweating, tachycardia, nausea, vomiting, syncope, murmur, and cyanosis. Pleurisy with friction rub may also be present. Arterial blood oxygen is frequently reduced. However, normal blood gases do not exclude PE. The erythrocyte sedimentation rate (ESR) is elevated in approximately 40% of patients, and electrocardiogram (ECG) may show right ventricle strain [47].

Chest X-ray is often normal in patients with pediatric PE. The signs such as atelectasis, pleural effusion, elevated hemidiaphragm, and infiltrate or consolidation are variable and not specific for PE. Oligemia distal to PE (Westermark sign) or a shallow, wedge-shaped opacity with its base against the pleura (Hampton hump) is not frequently seen [47]. CT pulmonary angiography (CTPA) can be performed quickly in critically ill patients. With the availability of CTA and its high sensitivity and specificity, pulmonary CTA is now more common procedure for the diagnosis of PE [48]. Pulmonary embolism appears as filling defects in the pulmonary arteries. A normal helical CT scan reduces the probability of pulmonary embolism; however, the use of iodinated contrast and the presence of radiation exposure are disadvantages of CTPA. If the patient has an allergy to iodinated contrast material or renal insufficiency or CTA is not available, a V/Q scan may be considered. Stein et al. suggest performing a V/Q if the chest radiograph is normal and acquiring CTA if there is an abnormality on the chest X-ray [49].

The radiopharmaceutical used for lung perfusion imaging is ^{99m}Tc-macroaggregated albumin (^{99m}Tc-MAA). After slow intravenous injection with the patient in a supine position, ^{99m}Tc-MAA particles lodge in pre-capillary arterioles, causing a temporary occlusion in a distribution proportional to regional arterial blood flow in lungs. The number of occluded arterioles by ^{99m}Tc-MAA particles is approximately 0.1% of their total number which is relatively small [50]. The particles clear by enzymatic hydrolysis and are eventually phagocytized by reticuloendothelial system and eliminated in the bile, with a biologic half-life in the lungs of between 6 and 8 h. The particle size is generally between 10 and 90 μm (90% of particles), with an average number of 500,000 particles in adult dose. In children, the number of particles should be adjusted to the age or weight to keep the number as low as possible in order to embolize no more than 0.1% of the total lung capillary vessels. It is estimated that neonates have about 10% of the eventual number of adult pulmonary capillaries. The number of capillaries increases to half of the adult value by age 3 years and reaches an adult level by age 8–12 years. The number of injected particles should not exceed 50,000 in the newborn and 165,000 for children at 1 year old. The recom-

mended number of particles for 5–10 years old with average weight of 20–35 kg is from 200,000 to 300,000 [50]. In infants and children with right-to-left shunt or pulmonary hypertension, the number of particles should be reduced (10,000–30,000 particles) depending on the age of the patient and the severity of involvement. The recommended dose by North American Consensus Guidelines is 2.59 MBq/kg (0.07 mCi/kg) if ^{99m}Tc is used for ventilation study and 1.11 MBq/kg (0.03 mCi/kg) if no concomitant ^{99m}Tc ventilation study is performed, with a minimum dose of 14.8 MBq (0.4 mCi) [20]. When administering ^{99m}Tc-MAA, withdrawing blood into the syringe should be avoided as small clots may occur with hot spots appearing on the images. If ^{99m}Tc-labeled radioaerosols or Technegas is used for the ventilation scan, this should be performed before the perfusion scan. If ^{81m}Kr gas is used for the ventilation scan, this can be acquired before or after the perfusion scan, or both examinations may be performed simultaneously as a dual-isotope scan [50].

Images can be acquired after radiotracer administration using a high-resolution, low-energy collimator. Planar images are obtained in a 128 × 128 or 256 × 256 matrix format, with a zoom large enough to include both lungs in the field of view with good margins. Multiple projections should be obtained including anterior, posterior, anterior and posterior oblique, and both lateral projections. SPECT or SPECT/CT study can also be performed. The CT portion is acquired with a low-dose CT for attenuation and anatomic correlation [50, 51].

^{99m}Tc-DTPA Aerosol: ^{99m}Tc-DTPA aerosol is the most commonly used radiopharmaceutical. Many different aerosols have been used, but DTPA is preferred in children because of the fast renal clearance, which lowers the radiation burden. ^{99m}Tc-DTPA aerosol can be inhaled through a mask connected to a nebulizer containing a saline solution of the radiopharmaceutical or preferably using a mouthpiece and nose clips in older children [50]. Swallowing of saliva may cause high gastric signal with possible difficult visualization of the left lower lung field. Cooperative children can be asked to rinse their mouth with water before beginning image acquisition. Aerosolized ^{99m}Tc-DTPA crosses the alveolar-capillary membrane and enters the bloodstream where it is then filtered by the kidneys. Increased permeability of alveolar-capillary membrane and thus lung clearance can be seen after exercise or certain lung disease such as cystic fibrosis.

Ventilation imaging is usually performed before perfusion imaging. Since both agents are labeled with ^{99m}Tc, it is extremely important that the count rate of the second study be at least three times the count rate of the first study. One advantage of ^{99m}Tc-DTPA aerosol is the persistence of activity in the lungs which allows for the acquisition of multiple projections or SPECT to match the perfusion images. Also, collection systems (required when using radioactive gases) are not necessary with the use of radioactive aerosols [50].

Xenon-133: Xenon is an inert gas with low solubility in body fluids and higher solubility in fat. After ^{133}Xe inhalation in single breath, the pattern of distribution reflects the regional ventilation. It has a physical half-life of 5.24 days and a low-energy gamma emission (81 keV). However, it rapidly washes out from the lungs with a half time of 5–30 s. The usual dose for children is 10–12 MBq/kg (0.3 mCi/kg) with a minimum dose of 100–120 MBq. The Xe-133 ventilation scan is generally performed prior to the Tc-99m MAA perfusion exam, as downscatter from the Tc-99m would severely degrade image quality. A posterior projection is generally used, while a bolus of ^{133}Xe is injected into the mouthpiece of the spirometer system at a time when the patient begins maximal inspiration. The imaging room should provide appropriate exhaust for radioactive gas. The advantage of a xenon exam is the ability to obtain single breath, equilibrium, and washout images providing better sensitivity and evaluation of ventilation in patients with obstructive lung disease [50].

Krypton-81m: ^{81m}Kr gas is produced by a rubidium generator (^{81}Rb/^{81m}Kr) with a half-life of 13 s and emission of a 190 keV gamma ray. The gas is administered by continuous inhalation mixed with atmospheric air during the acquisition

of the images. Because it has a short half-life, Krypton-81m is not considered an environmental hazard, and storage or exhaust systems are not necessary. The radiation dose to the lungs is lower than with other agents. However, the generator is expensive and can be used only for one working day which makes it impractical for most clinical situations. In addition, it is currently not available in the United States [51].

Several diagnostic schemes have been suggested for interpretation of V/Q scans, such as the modified PIOPED II with the proposed criteria for a very low probability interpretation to improve the accuracy and minimize the number of nonconclusive results [52]. However, in the daily practice of nuclear medicine, experienced physicians may not follow a strict single interpretive criteria but rather use integrated knowledge of different published criteria and their own experience ("Gestalt" interpretation) [53]. Several studies were performed to evaluate the performance of different readers with different experience using different widespread algorithms such as PIOPED criteria, earlier schemes developed by McNeil and Biello. In general, the ideal scheme would minimize the frequency of intermediate or indeterminate results. Glaser et al. suggested a trinary interpretation for V/Q scanning considering normal, very low probability, and low probability read as no evidence of PE, high probability as PE present, and intermediate probability as nondiagnostic [54]. Single segmental mismatches were considered positive for PE. The trinary interpretation group included 664 examinations, with 8.4% being PE present, 3.5% nondiagnostic, and 88.1% PE negative. Pediatric subgroup analysis in 20 children showed positive in 10%, nondiagnostic in 5%, and negative in 85%, with no false negatives using either scheme. They concluded that the trinary interpretation can safely be used. In children, Gelfand et al. evaluated the frequency of indeterminate findings in children without known lung disease or previous extensive PE and reported a low rate of indeterminate studies using criteria of Biello et al. with minimal modification. It was concluded that V/Q scans are still appropriate for imaging children with suspected PE [55].

27.17 Thyroid Scan for Congenital Hypothyroidism

Thyroid hormone deficiency at birth is most commonly caused by a problem with thyroid gland development (dysgenesis), including ectopic thyroid tissue, no thyroid tissue (athyreosis), and less frequently hypoplasia, or a disorder of thyroid hormone biosynthesis (dyshormonogenesis). These disorders result in primary hypothyroidism [90]. Thyroid dysgenesis is generally sporadic, but thyroid dyshormonogenesis is associated with hormone synthesis protein gene mutations [91].

Congenital hypothyroidism (CH) is classified into two main types: transient and permanent. Permanent CH is mainly due to primary hypothyroidism presented with elevated thyroid-stimulating hormone (TSH) levels. Transient hypothyroidism can be due to maternal antithyroid medications, transplacental thyrotropin receptor blocking antibodies, and iodine imbalance (deficiency or excess) as well as genetic defects such as mutations in the genes encoding for DUOX and DUOXA2 [90].

The incidence of CH initially increased after the introduction of newborn screening with a range of 1:3000 to 1:4000. However, recent reports showed that the incidence is increased with rates ranging from 1:1400 to 1:2800 in many countries. The rise in incidence could be attributed to the change in demographics, change in newborn screening strategies such as lowering cutoff values, and increase in preterm birth [92]. A higher incidence was reported in the Asian, Native American, and Hispanic populations and lower in the African American population. It is more common in females with approximately a 2:1 female to male ratio [90]. Early treatment with thyroid hormone replacement is essential for normal neurodevelopment. The treatment should be started once the diagnosis is confirmed based on serum thyroid function test results [90].

Diagnostic studies may be performed to determine an underlying etiology. These include thyroid scintigraphy, thyroid ultrasonography, serum thyroglobulin (Tg) measurement, antithyroid antibody determinations, and measurement of

urinary iodine. Thyroid imaging can be helpful in differentiating underlying etiology (either thyroid dysgenesis or dyshormonogenesis).

Iodine-123 (^{123}I) or sodium pertechnetate-99m (^{99m}Tc) can be used for thyroid imaging. Iodine-131 (^{131}I) is not recommended due to higher radiation dose to the thyroid. ^{99m}Tc is taken up by the thyroid through sodium–iodine symporter (NIS) but unlike iodine is not organified. More prominent physiologic activity in salivary glands is seen in ^{99m}Tc compared to iodine scans. ^{99m}Tc is commonly used due to its availability, lower cost, and faster exam times. The intravenous administered dose for children is 1.1 MBq/kg with a minimum dose of 7 MBq [93]. Imaging is started 20 min after injection. Static images with the neck extended can be obtained for 5 min. Anterior views of the neck and thorax are acquired using a low-energy high-resolution collimator and a 128 × 128 matrix. Lateral views can be acquired with a chin marker for better anatomic localization [94].

Unlike ^{99m}Tc, ^{123}I is organified and then incorporated into thyroid hormones. The administered dose is 0.28 MBq/kg with a minimum dose of 1 MBq [93]. Imagining can be acquired 2–4 h after administration. ^{123}I is the preferred agent particularly if a perchlorate discharge test is required for dyshormonogeneses in children with eutopic thyroid. If there is defective organification of iodide, the uptake in the thyroid gland will be decreased by more than 10% when perchlorate is given [94]. However, ^{123}I is more expensive and less readily available and requires a longer time to complete.

Absent thyroid activity is likely to represent athyreosis (Fig. 27.16). Ultrasound can be performed to confirm the diagnosis as absence of uptake can also be seen with TSHβ gene mutations, TSH receptor-inactivating mutations, iodide trapping defects, and maternal thyrotropin receptor blocking antibodies [90].

Ectopic activity in a thyroid scan can be found along the embryological migration pathway from the foramen cecum at the base of the tongue to the mediastinum. Lingual thyroid is typically presented with small focus of uptake in the midline at the base of the tongue

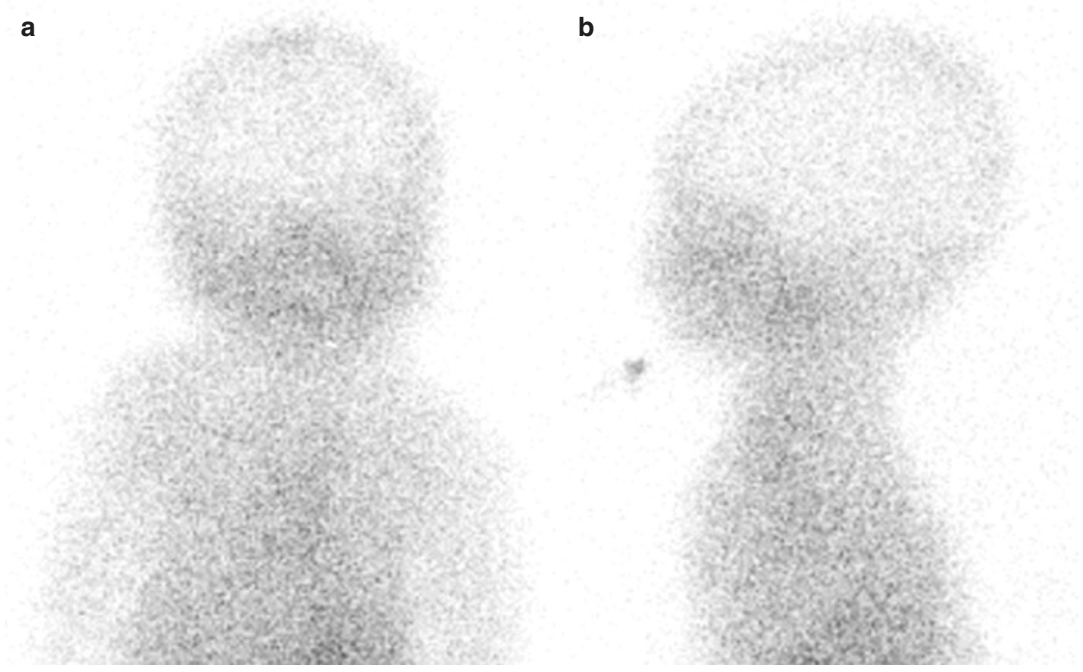

Fig. 27.16 Thyroid agenesis congenital hypothyroidism: thyroid scan (**a**, anterior; **b**, lateral) in a 4-day-old boy with congenital hypothyroidism shows no activity in the thyroid bed suggestive of agenesis or a suppressed thyroid

(Fig. 27.17). In hypoplasia, the uptake is usually low in the thyroid gland and could be unilateral causing asymmetric uptake [94].

In dyshormonogenesis, a patient may present with a palpable goiter. The thyroid scan may demonstrate an enlarged gland in eutopic location with increased uptake, suggesting dyshormonogeneses beyond trapping (Fig. 27.18). I-123 uptake can be followed by a perchlorate discharge test [95].

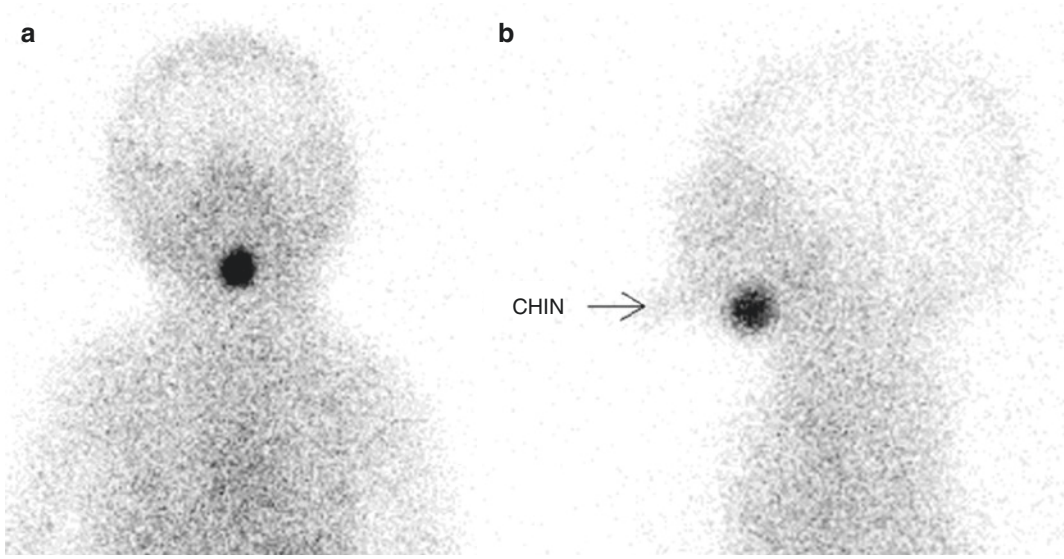

Fig. 27.17 Lingual thyroid; thyroid scan (**a**, anterior; **b**, lateral) in a 7-day-old infant with congenital hypothyroidism shows a focal activity at the base of the tongue

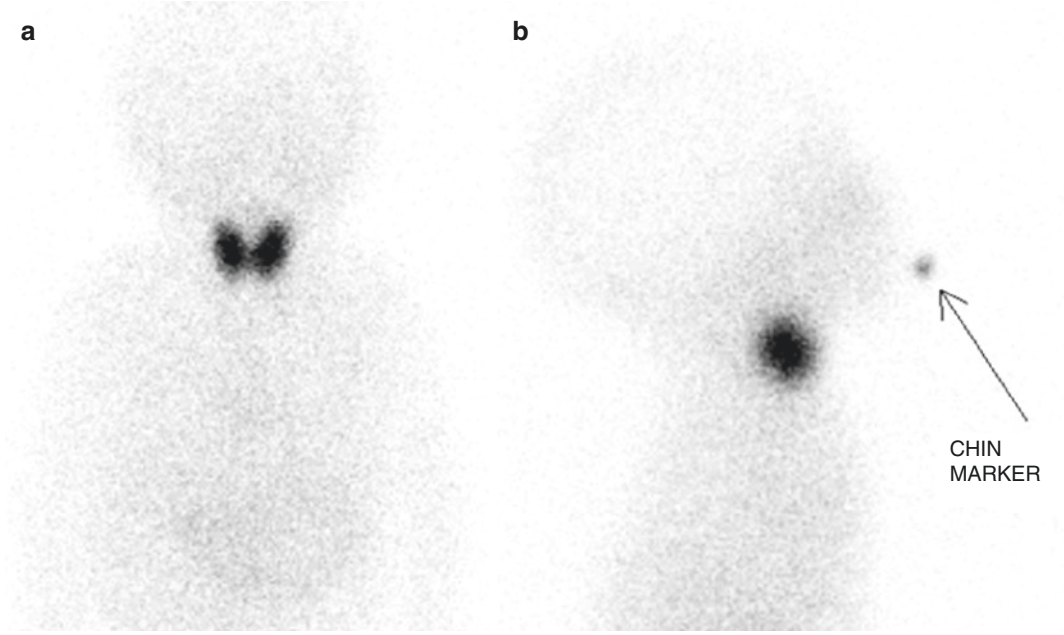

Fig. 27.18 Dyshormonogenesis: thyroid scan (**a**, anterior; **b**, lateral) in a 6-day-old infant with congenital hypothyroidism shows marked increased activity in both thyroid lobes suggestive of organification enzyme defect (dyshormonogenesis)

References

1. Stabin MG, Gelfand MJ. Dosimetry of pediatric nuclear medicine procedures. Q J Nucl Med. 1998;42(2):93–112.
2. Gordon I, Piepsz A, Sixt R. Guidelines for standard and diuretic renogram in children; guideline. Eur J Nucl Med Mol Imaging. 2011;38:1175.
3. Shulkin BL, Mandell GA, Cooper JA, et al. Procedure guideline for diuretic renography in children 3.0. J Nucl Med Technol. 2008;36(3):162–8.
4. Chotipanich C, Rubin J, Lin J, Charron M. Clinical follow-up of children with low differential function on diuretic renogram. J Med Assoc Thai. 2007;90(4):754–61.
5. Mandell G, Eggli D, Gilday D, et al. Society of nuclear medicine procedure guideline for renal cortical scintigraphy in children version 3.0. Approved June 20, 2003.
6. Ajdinovic B, Jaukovic L, Krstic Z, Dopuda M. Impact of micturating cystourethrography and DMSA renal scintigraphy on the investigation scheme in children with urinary tract infection. Ann Nucl Med. 2008;22(8):661–5.
7. Hoberman A, Charron M, Hickey RW, Baskin M, Kearney DH, Wald ER. Imaging studies after a first febrile urinary tract infection in young children. N Engl J Med. 2003;348(3):195–202.
8. Lim R. Vesicoureteral reflux and urinary tract infection: evolving practices and current controversies in pediatric imaging. AJR Am J Roentgenol. 2009;192(5):1197–208.
9. Pollet JE, Sharp PF, Smith FW. Radionuclide imaging for vesico-renal reflux using intravenous 99mTc--D.T.P.A. Pediatr Radiol. 1979;8(3):165–7.
10. Gerhold JP, Klingensmith WC III, Kuni CC, et al. Diagnosis of biliary atresia with radionuclide hepatobiliary imaging. Radiology. 1983;146(2):499–504.
11. Warrington JC, Charron M. Pediatric gastrointestinal nuclear medicine. Semin Nucl Med. 2007;37(4):269–85.
12. Donohoe KJ, Maurer AH, Ziessman HA, et al. Procedure guideline for adult solid-meal gastric-emptying study 3.0. J Nucl Med Technol. 2009;37(3):196–200.
13. Fawcett HD, Hayden CK, Adams JC, Swischuk LE. How useful is gastroesophageal reflux scintigraphy in suspected childhood aspiration? Pediatr Radiol. 1988;18(4):311–3.
14. Siegel J, Wu R, Knight L, Zelac R, Stern H, Malmud L. Radiation dose estimates for oral agents used in upper gastrointestinal disease. J Nucl Med. 1983;24:835–37.
15. Baikie G, South MJ, Reddihough DS, et al. Agreement of aspiration tests using barium videofluoroscopy, salivagram, and milk scan in children with cerebral palsy. Dev Med Child Neurol. 2005;47(2):86–93.
16. Sonneville A, Ait-Tahar H, Baulieu F, et al. [Value of esophageal scintigraphy in exploration of a gastro-esophageal reflux in a respiratory patient]. Allerg Immunol 2000;32(5):207–208.
17. Sfakianakis GN, Conway JJ. Detection of ectopic gastric mucosa in Meckel's diverticulum and in other aberrations by scintigraphy: II. Indications and methods–a 10-year experience. J Nucl Med. 1981;22(8):732–8.
18. Spottswood SE, Pfluger T, Bartold S, et al. SNMMI and EANM Practice Guideline for meckel diverticulum scintigraphy. J Nucl Med Technol. 2014;42(3):163–9.
19. Vali R, Daneman A, McQuattie S, Shammas A. The value of repeat scintigraphy in patients with a high clinical suspicion for Meckel diverticulum after a negative or equivocal first Meckel scan. Pediatr Radiol. 2015;45:1506–14.
20. Gelfand MJ, Parisi MT, Treves ST, Pediatric Nuclear Medicine Dose Reduction Workgroup. Pediatric radiopharmaceutical administered doses: 2010 North American consensus guidelines. J Nucl Med. 2011;52(2):318–22.
21. Lassmann M, Treves ST, EANM/SNMMI Paediatric Dosage Harmonization Working Group. Paediatric radiopharmaceutical administration: harmonization of the 2007 EANM paediatric dosage card (version 1.5.2008) and the 2010 North American consensus guidelines. Eur J Nucl Med Mol Imaging. 2014;41(5):1036–41.
22. Grant FD. 18F-Fluoride PET and PET/CT in children and young adults. PET Clin. 2014;9(3):287–97.
23. Nadel HR. Pediatric bone scintigraphy update. Semin Nucl Med. 2010;40(1):31–40.
24. De Palma D. Radionuclide studies with bone-seeking radiophamaceuticals in pediatric benign diseases. In: Mansi L, et al., editors. Clinical nuclear medicine in pediatrics. New York, NY: Springer; 2016.
25. Ma JJ, Kang BK, Treves ST. Pediatric musculoskeletal nuclear medicine. Semin Musculoskelet Radiol. 2007;11(4):322–34.
26. De Palma D, Nadel HR, Bar-Sever Z. Skeletal scintigraphy with SPECT/CT in benign pediatric bone conditions. Clin Transl Imag. 2016;4:191.
27. Bybel B, Brunken RC, DiFilippo FP, et al. SPECT/CT imaging: clinical utility of an emerging technology. Radiographics. 2008;28(4):1097–113.
28. Treves ST. Skeletal scintigraphy: general considerations. In: Treves ST, editor. Pediatric nuclear medicine and molecular imaging. 4th ed. New York, NY: Springer; 2014.
29. Faden H, Grossi M. Acute osteomyelitis in children. Reassessment of etiologic agents and their clinical characteristics. Am J Dis Child. 1991;145(1):65–9.
30. Connolly LP, Drubach SA, Connolly SA, et al. Bone. In: Treves ST, editor. Pediatric nuclear medicine/PET. 3rd ed. New York, NY: Springer; 2007.
31. Schauwecker DS. The scintigraphic diagnosis of osteomyelitis. AJR Am J Roentgenol. 1992;158(1):9–18.
32. Pennington WT, Mott MP, Thometz JG, et al. Photopenic bone scan osteomyelitis: a clinical perspective. J Pediatr Orthop. 1999;19(6):695–8.
33. Acikgoz G, Averill L. Chronic recurrent multifocal osteomyelitis: typical patterns of bone involvement in whole-body bone scintigraphy. Nucl Med Commun. 2014;35(10):1097.

34. Connolly LP, Treves ST. Assessing the limping child with skeletal scintigraphy. J Nucl Med. 1998;39(6):1056–61.
35. Drubach LA, Connolly LP, D'Hemecourt PA, et al. Assessment of the clinical significance of asymptomatic lower extremity uptake in young athletes. J Nucl Med. 2001;42(2):209–12.
36. Sty JR, Wells RG, Conway JJ. Spine pain in children. Semin Nucl Med. 1993;23(4):296–320.
37. Pekindil G, Sarikaya A, Pekindil Y, et al. Lumbosacral transitional vertebral articulation: evaluation by planar and SPECT bone scintigraphy. Nucl Med Commun. 2004;25(1):29–37.
38. Mandelstam SA, Cook D, Fitzgerald M, et al. Complementary use of radiological skeletal survey and bone scintigraphy in detection of bony injuries in suspected child abuse. Arch Dis Child. 2003;88(5):387–90.
39. Conway JJ, Collins M, Tanz RR, et al. The role of bone scintigraphy in detecting child abuse. Semin Nucl Med. 1993;23(4):321–33.
40. Drubach LA, Johnston PR, Newton AW, et al. Skeletal trauma in child abuse: detection with 18F-NaF PET. Radiology. 2010;255(1):173–81.
41. Villani MF, Falappa P, Pizzoferro M, Toniolo RM, Lembo A, Chiapparelli S, Garganese MC. Role of three-phase bone scintigraphy in paediatric osteoid osteoma eligible for radiofrequency ablation. Nucl Med Commun. 2013;34(7):638–44.
42. Zhibin Y, Quanyong L, Libo C, et al. The role of radionuclide bone scintigraphy in fibrous dysplasia of bone. Clin Nucl Med. 2004;29:177–80.
43. Connolly LP, Drubach LA, Treves ST. Pediatric skeletal scintigraphy. In: Henkin RE, Bova D, Dillehay GL, Karesh SM, Halama JR, Wagner RH, editors. Nuclear medicine. 2nd ed. Philadelphia, PA: Mosby-Elsevier; 2006. p. 1721–44.
44. Stauss J, Hahn K, Mann M, De Palma D. Guidelines for paediatric bone scanning with 99mTc-labelled radiopharmaceuticals and 18F-fluoride. Eur J Nucl Med Mol Imaging. 2010;37(8):1621–8.
45. Patocka C, Nemeth J. Pulmonary embolism in pediatrics. J Emerg Med. 2012;42(1):105–16.
46. Buck JR, Connors RH, Coon WW, et al. Pulmonary embolism in children. J Pediatr Surg. 1981;16(3):385–91.
47. Brandão LR, Labarque V, Diab Y, et al. Pulmonary embolism in children. Semin Thromb Hemost. 2011;37(7):772–85.
48. Hunt JM, Bull TM. Clinical review of pulmonary embolism: diagnosis, prognosis, and treatment. Med Clin North Am. 2011;95(6):1203–22.
49. Stein EG, Haramati LB, Chamarthy M, Sprayregen S, Davitt MM, Freeman LM. Success of a safe and simple algorithm to reduce use of CT pulmonary angiography in the emergency department. AJR Am J Roentgenol. 2010;194(2):392–7.
50. Ciofetta G, Piepsz A, Roca I, et al. Guidelines for lung scintigraphy in children. Eur J Nucl Med Mol Imaging. 2007;34(9):1518–26.
51. Parker JA, Coleman RE, Grady E, et al. SNM practice guideline for lung scintigraphy 4.0. J Nucl Med Technol. 2012;40(1):57–65.
52. Gottschalk A, Stein PD, Sostman HD, et al. Very low probability interpretation of V/Q lung scans in combination with low probability objective clinical assessment reliably excludes pulmonary embolism: data from PIOPED II. J Nucl Med. 2007;48(9):1411–5.
53. Shammas A, Vali R, Charron M. Pediatric Nuclear Medicine in Acute Care. Semin Nucl Med. 2013;43(2):139–56.
54. Glaser JE, Chamarthy M, Haramati LB, et al. Successful and safe implementation of a trinary interpretation and reporting strategy for V/Q lung scintigraphy. J Nucl Med. 2011;52(10):1508–12.
55. Gelfand MJ, Gruppo RA, Nasser MP. Ventilation-perfusion scintigraphy in children and adolescents is associated with a low rate of indeterminate studies. Clin Nucl Med. 2008;33(9):606–9.
56. Bodei L, Lam M, Chiesa C, et al. EANM procedure guideline for treatment of refractory metastatic bone pain. Eur J Nucl Med Mol Imaging. 2008;35(10):934–1940.
57. Olivier P, Colarinha P, Fettich J, et al. Guidelines for radioiodinated MIBG scintigraphy in children. Eur J Nucl Med Mol Imaging. 2003;30(5):B45–50.
58. Kowalsky RJ, Falen SW. Radiopharmaceuticals in nuclear pharmacy and nuclear medicine. 2nd ed. Washington DC: American Pharmacists Association; 2004.
59. Lonergan GJ, Schwab CM, Suarez ES, et al. Neuroblastoma, ganglioneuroblastoma, and ganglioneuroma: radiologic-pathologic correlation. Radiographics. 2002;22(4):911–34.
60. Bombardieri E, Giammarile F, Aktolun C, et al. 131I/123I-Metaiodobenzylguanidine (mIBG) scintigraphy: procedure guidelines for tumour imaging. Eur J Nucl Med Mol Imaging. 2010;37:2436–46.
61. Boubaker A, Bischof Delaloye A. Nuclear medicine procedures and neuroblastoma in childhood. Their value in the diagnosis, staging and assessment of response to therapy. Q J Nucl Med. 2003;47(1):31–40.
62. Alexander N, Vali R, Ahmadzadehfar H, Shammas A, Baruchel S. Review: the role of radiolabeled DOTA-conjugated peptides for imaging and treatment of childhood neuroblastoma. Curr Radiopharm. 2018;11(1):14–21.
63. Zhang L, Vines D, Scollard D, et al. Correlation of somatostatin receptor-2 expression with gallium-68-DOTA-TATE uptake in neuroblastoma xenograft models. Contrast Media Mol Imaging. 2017;2017:9481276.
64. Barthlen W, Mohnike W, Mohnike K. Techniques in pediatric surgery: congenital hyperinsulinism. Horm Res Paediatr. 2010;74:438–43.
65. Arnoux JB, de Lonlay P, et al. Congenital hyperinsulinism. Early Hum Dev. 2010;86:287–94.
66. McAndrew HF, Smith V, et al. Surgical complications of pancreatectomy for persistent hyperinsulinaemic hypoglycaemia of infancy. J Pediatr Surg. 2003;38:13–6. discussion 13–16.

67. McCarville M. PET-CT imaging in pediatric oncology. Cancer Imaging. 2009;9(1):35–43.
68. Krohmer S, Sorge I, Krausse A, Kluge R, Bierbach U, Marwede D, et al. Whole-body MRI for primary evaluation of malignant disease in children. Eur J Radiol. 2010;74(1):256–261.6.
69. Volker T, Denecke T, Steffen I, Misch D, Schonberger S, Plotkin M, et al. Positron emission tomography for staging of pediatric sarcoma patients: results of a prospective multicenter trial. J Clin Oncol. 2007;25(34):5435–41.
70. Bisdas S, Ritz R, Bender B, Braun C, Pfannenberg C, Reimold M, et al. Metabolic mapping of gliomas using hybrid MR-PET imaging: feasibility of the method and spatial distribution of metabolic changes. Invest Radiol. 2013;48(5):295–301.
71. Warbey VS, Ferner RE, Dunn JT, Calonje E, O'Doherty MJ. [^{18}F] FDG PET/CT in the diagnosis of malignant peripheral nerve sheath tumours in neurofibromatosis type-1. Eur J Nucl Med Mol Imaging. 2009;36(5):751–7.
72. Gatidis S, Schmidt H, Gucke B, Bezrukov I, Seitz G, Ebinger M, et al. Comprehensive oncologic imaging in infants and preschool children with substantially reduced radiation exposure using combined simultaneous ^{18}F-fluorodeoxyglucose positron emission tomography/magnetic resonance imaging: a direct comparison to ^{18}F fluorodeoxyglucose positron emission tomography/computed tomography. Invest Radiol. 2016;51(1):7–14.
73. Schafer JF, Gatidis S, Schmidt H, Guckel B, Bezrukov I, Pfannenberg CA, et al. Simultaneous whole-body PET/MR imaging in comparison to PET/CT in pediatric oncology: initial results. Radiology. 2014;273(1):220–31.
74. Nihayah S, Shammas A, Vali R, Parra D, Alexander S, Amaral J, Connolly B. Correlation of PET/CT and image-guided biopsies of pediatric malignancies. AJR Am J Roentgenol. 2017;208(3):656–62.
75. Blokhuis GJ, Bleeker-Rovers CP, Diender MG, Oyen WJ, Draaisma JM, de Geus-Oei LF. Diagnostic value of FDG-PET/(CT) in children with fever of unknown origin and unexplained fever during immune suppression. Eur J Nucl Med Mol Imaging. 2014;41(10):1916–23.
76. Ferdinand B, Gupta P, Kramer EL. Spectrum of thymic uptake at 18F-FDG PET. Radiographics. 2004;24(6):1611–6.
77. Sasaki M, Kuwabara Y, Ichiya Y, et al. Differential diagnosis of thymic tumors using a combination of 11C-methionine PET and FDG PET. J Nucl Med. 1999;40(10):1595–601.
78. Bemben MG, Massey BH, Bemben DA, et al. Age-related variability in body composition methods for assessment of percent fat and fat-free mass in men aged 20–74 years. Age Ageing. 1998;27(2):147–53.
79. Delbeke D, Coleman R, Milton J, et al. Procedure guideline for tumor imaging with 18F-FDG PET/CT 1.0. In: SNM guideline. Reston, VA: SNM; 2006.
80. Nakagawa TA, Ashwal S, Mathur M, et al. Guidelines for the determination of brain death in infants and children: an update of the 1987 Task Force recommendations. Crit Care Med. 2011;39(9):2139–55.
81. Banasiak KJ, Lister G. Brain death in children. Curr Opin Pediatr. 2003;15(3):288–93.
82. Friedman NC, Burt RW. Cerebral perfusion imaging. In: Henkin RE, Bova D, Dillehay GL, et al., editors. Nuclear medicine. 2nd ed. Philadelphia, PA: Mosby-Elsevier; 2006.
83. Donohoe KJ, Agrawal G, Frey KA, et al. SNM practice guideline for brain death scintigraphy 2.0. J Nucl Med Technol. 2012;40(3):198–203.
84. Okuyaz C, Gücüyener K, Karabacak NI, et al. Tc-99m-HMPAO SPECT in the diagnosis of brain death in children. Pediatr Int. 2004;46(6):711–4.
85. Sinha P, Conrad GR. Scintigraphic confirmation of brain death. Semin Nucl Med. 2012;42(1):27–32.
86. Coker SB, Dillehay GL. Radionuclide cerebral imaging for confirmation of brain death in children: the significance of dural sinus activity. Pediatr Neurol. 1986;2(1):43–6.
87. Wieler H, Marohl K, Kaiser KP, et al. Tc-99m HMPAO cerebral scintigraphy. A reliable, noninvasive method for determination of brain death. Clin Nucl Med. 1993;18:104–9.
88. Facco E, Zucchetta P, Munari M, Baratto F, et al. 99mTc-HMPAO SPECT in the diagnosis of brain death. Intensive Care Med. 1998;24(9):911–7.
89. Ashwal S, Schneider S. Brain death in the newborn. Pediatrics. 1989;84(3):429–37.
90. Rastogi MV, LaFranchi SH. Congenital hypothyroidism. Orphanet J Rare Dis. 2010;5:17. https://doi.org/10.1186/1750-1172-5-17.
91. Léger J, Olivieri A, Donaldson M, Torresani T, Krude H, van Vliet G, et al. European Society for Paediatric Endocrinology consensus guidelines on screening, diagnosis, and management of congenital hypothyroidism. J Clin Endocrinol Metab. 2014;99:363 84.
92. Wassner AJ, Brown RS. Congenital hypothyroidism: recent advances. Curr Opin Endocrinol Diabetes Obes. 2015;22(5):407–12.
93. Treves ST, Gelfand MJ, Fahey FH, Parisi MT. 2016 Update of the North American Consensus Guidelines for pediatric administered radiopharmaceutical activities. J Nucl Med. 2016;57(12):15N–8N.
94. Keller-Petrot I, Leger J, Sergent-Alaoui A, de Labriolle-Vaylet C. Congenital hypothyroidism: role of nuclear medicine. Semin Nucl Med. 2017;47(2):135–42.
95. Volkan-Salancı B, Özgen Kıratlı P. Nuclear medicine in thyroid diseases in pediatric and adolescent patients. Mol Imaging Radionucl Ther. 2015;24(2):47–59. https://doi.org/10.4274/mirt.76476.